NEURAL CIRCUITS FACILITATING SIGNAL DETECTION IN THE AUDITORY CORTEX

by

ANNA ANDREEVNA LAKUNINA

A DISSERTATION

Presented to the Department of Biology
and the Division of Graduate Studies of the University of Oregon
in partial fulfillment of the requirements
for the degree of
Doctor of Philosophy

June 2021

DISSERTATION APPROVAL PAGE

Student: Anna Andreevna Lakunina

Title: Neural Circuits Facilitating Signal Detection in the Auditory Cortex

This dissertation has been accepted and approved in partial fulfillment of the requirements for the Doctor of Philosophy degree in the Department of Biology by:

Matthew Smear	Chair
Santiago Jaramillo	Advisor
Shawn Lockery	Core Member
Yashar Ahmadian	Core Member
Michael Wehr	Institutional Representative

and

Andrew Karduna	Interim Vice Provost for Graduate Studies

Original approval signatures are on file with the University of Oregon Division of Graduate Studies.

Degree awarded June 2021

DISSERTATION ABSTRACT

Anna Andreevna Lakunina

Doctor of Philosophy

Department of Biology

June 2021

Title: Neural Circuits Facilitating Signal Detection in the Auditory Cortex

The natural acoustic environment is very noisy, with sounds coming from many sources and containing many overlapping frequency components. To navigate this environment, it is necessary for animals to be able to decompose this auditory stream of information into behaviorally relevant signals and irrelevant background noise. However, the mechanisms by which this separation takes place in the auditory system is not fully understood. In this dissertation, I investigated the role of auditory cortical circuits in signal detection. In Chapter II, I describe our findings that somatostatin-expressing inhibitory interneurons mediate spectral surround suppression, a form of global integration that may be useful for suppression of responses to broadband noise. In Chapter III, I found that the auditory cortex plays an important role in the perception of stimuli immersed in noise, and that perturbation of inhibitory interneurons reduces an animal's ability to detect a masked signal. Together, these works expand our knowledge of the neural computations taking place in the sensory cortex that allow for the separation of signals from noise.

This dissertation includes previously published co-authored material.

CURRICULUM VITAE

NAME OF AUTHOR: Anna Andreevna Lakunina

GRADUATE AND UNDERGRADUATE SCHOOLS ATTENDED:

University of Oregon, Eugene
University of Washington, Seattle

DEGREES AWARDED:

Doctor of Philosophy, Biology, 2021, University of Oregon
Bachelor of Science, Neurobiology, 2012, University of Washington
Bachelor of Science, Mathematics, 2012, University of Washington

AREAS OF SPECIAL INTEREST:

- Neural basis of behavior
- Sensory coding
- Circuit mechanisms of neural computations
- High-density extracellular electrophysiology
- Calcium imaging

PROFESSIONAL EXPERIENCE:

Graduate Research Assistant
Graduate Teaching Assistant

PUBLICATIONS:

A.A. Lakunina, M.B. Nardoci, Y. Ahmadian, S. Jaramillo (2020). Somatostatin-expressing interneurons in the auditory cortex mediate sustained suppression by spectral surround. *Journal of Neuroscience.* 40(18):3564-3575.

ACKNOWLEDGEMENTS

Thank you to Santiago and every member of the Jaramillo lab, past and present, for all the support you have given me and my projects over the course of my dissertation. Thank you also to my committee, who has supported me during my work at the UO and helped me in establishing my path after. Further thanks goes to the ION community at large and to the ION support staff, who helped me when the going got tough.

I would also like to thank the staff of UO's core facilities, who are often overlooked despite how essential they are to our research endeavours. Thank you to Kathy Snell and the staff of the Terrestrial Animal Care Services, without whom our lab would not be able to maintain our current colony and maintain our level of experimental throughput. Thank you also to the Histology and Genetic Modification Core Facility, particularly Leah DeBlander, whose assistance has been invaluable to my research.

TABLE OF CONTENTS

LIST OF FIGURES

Figure Page

CHAPTER I

INTRODUCTION

Our auditory environments are highly complex, with sound stimuli coming from many sources and comprised of many, often overlapping, frequency components. Despite this, the healthy auditory system is easily able to parse this deluge of sensory information into distinct auditory objects, even separating relevant stimuli from background noise. This latter ability is is often affected by age, injury, and neurological disease, resulting in hearing deficits in noisy environments that are not fully alleviated by current treatments like hearing aids (Ralli et al., 2019). The nervous system can use one of two methods to extract signals from noisy environments: (1) selective attention to currently relevant stimulus features, or (2) pre-attentive mechanisms to emphasize common features of natural signals. This dissertation will focus on the implementation of the latter processes within the primary auditory cortex. A deeper understanding of the auditory cortical populations important to performing signal-in-noise detection would allow us to implement such mechanisms in artificial systems and aid those with difficulty hearing.

I.1. Global integration of local stimulus features

We experience the acoustic world as a set of coherent auditory objects even though sensory organs in our ears detect the individual frequency components of sound. This implies the existence of mechanisms in the auditory system for integrating information across frequency channels to create global percepts (Metherate et al., 2005). Such global integration is necessary to identify behaviorally relevant sound stimuli and dismiss background noise. Responses to auditory

stimuli become increasingly noise-invariant in the ascending auditory pathway, with responses in the peripheral auditory system being most perturbed by the inclusion of noise, and responses in the auditory cortex faithfully representing the stimulus despite background noise (Mesgarani et al., 2014; Carruthers et al., 2015). To achieve this high level of noise-invariance, the auditory cortex could take advantage of typical statistics of natural sounds to differentiate stimulus features likely to be seen in a relevant auditory signal rather than background noise. For instance, noise-invariant responses to bird song in avian auditory areas can be achieved by selectively responding to spectro-temporal features characteristic of song (Moore et al., 2013). Conversely, natural background noise tends to contain power in many frequency bands that is co-modulated (Nelken et al., 1999). While there is evidence of cortical mechanisms emphasizing common features of signals and de-emphasizing or removing common features of noise, it is not fully understood how these mechanisms are implemented.

The cortex is highly interconnected with many horizontal connections between horizontal columns (Boucsein et al., 2011). As a result, a plausible mechanism for global integration of auditory stimuli could be long-range interactions across frequency channels that suppress noise but not signals. Indeed, the auditory cortex is known to be globally tonotopically organized and contain horizontal connections across cortical columns tuned to different frequencies (Kanold et al., 2014). Because achieving noise-invariant responses to signals requires suppression of responses to acoustic noise, cortical inhibition likely plays a role.

Cortical inhibitory interneurons can be categorized into different, non-overlapping classes based on their morphology, connectivity, and gene expression (Pfeffer et al., 2013; Kepecs and Fishell, 2014). The two most common types

of cortical inhibitory neurons are parvalbumin-expressing (PV^+) neurons, and somatostatin-expressing (SOM^+) neurons, which, together, comprise about 70% of cortical inhibitory neurons (Rudy et al., 2011). These two neuron types are known to have different response properties to auditory stimuli (Moore and Wehr, 2013; Li et al., 2015), as well as different patterns of connectivity to other cortical neurons (Kwan and Dan, 2012; Li et al., 2014). SOM^+ cells in particular have been shown to play a key role in producing network suppression that underlies lateral inhibition (Kato et al., 2017). This points to SOM^+ cells playing a unique role in facilitating global integration via their long-range influence in the auditory cortex, though the behavioural relevance of these connections is not currently known.

I.2. Global integration in the auditory cortex could affect perception of noisy stimuli

Navigating a noisy natural environment requires the ability to separate background noise from relevant signals to be able to detect and act on these signals. Previous research in tone-in-noise detection have focused on responses at the level of the auditory nerve, finding some degree of noise invariance in fibres tuned to the test frequency (Abbas, 1981; Costalupes, 1985). This research, however, assumes completely independent frequency channels and fails to account for the suppression of co-modulated noise that spans many frequencies. More recent research has shown an increase in noise invariance in higher auditory areas that corresponds to behavioural thresholds of signal detection (Schneider and Woolley, 2013). Models have been created to propose that temporal and spectral cues may be used to separate auditory signal from noise, though a physiological implementation of these models was not explored (Berg, 2004; Mao and Carney, 2015). Global integration across frequency

channels as it occurs in the auditory cortex could be a plausible mechanism by which animals filter out broadband environmental noise in order to better focus on behaviourally relevant signals.

I.3. How are global integration and signal detection implemented in the auditory cortex?

Previous studies of responses in the auditory cortex have shown that a subset of neurons show a decrease in response when the bandwidth of the sound stimulus is increased (Rauschecker and Tian, 2004; O'Connor et al., 2010; Li et al., 2019). This suppression in response to the addition of frequency components outside a cell's classical tonal receptive field is a form of global integration whose mechanism is not currently known. The similarity between this spectral surround suppression and the surround suppression observed in the visual cortex implies the existence of a common cortical motif that may be used to suppress noise (Adesnik et al., 2012). As such, I hypothesized that surround suppression may be implemented similarly in the visual and auditory cortices. In **Chapter II**, I investigate the extent to which auditory cortical neurons are surround suppressed, and determine whether this varies by cell type, hypothesizing that excitatory cells show a greater degree of surround suppression than inhibitory cells. Furthermore, I will determine the contributions of each inhibitory cell type to the observed surround suppression, and create a simple model of the response tuning of excitatory cells as a function of their thalamic and inhibitory inputs.

While Chapter II will focus on determining the mechanism for a form of global integration that takes place in the auditory cortex, in **Chapter III**, I investigate the neural correlates of auditory signal detection. Auditory stimuli are encoded on the

population-level in the primary auditory cortex even when masked by broadband noise (Carcea et al., 2017), implying some form of processing has taken place by that level to filter out responses to background noise. I hypothesize that spectral surround suppression is one such form of processing and may aid in signal detection by suppressing responses to broadband noise and enhancing responses to narrowband signals like pure tones. As such, I expect that the sources of inhibition that have the most dominant contributions to surround suppression also have the greatest effect on behavioural signal detection.

CHAPTER II

SOMATOSTATIN-EXPRESSING INTERNEURONS IN THE AUDITORY CORTEX MEDIATE SUSTAINED SUPPRESSION BY SPECTRAL SURROUND

II.1. Author contributions

Originally published as: A.A. Lakunina, M.B. Nardoci, Y. Ahmadian, S. Jaramillo (2020). Somatostatin-expressing interneurons in the auditory cortex mediate sustained suppression by spectral surround. Journal of Neuroscience. 40(18):3564-3575. AAL, YA, and SJ conceived the project and designed the experiments. AAL and MBN conducted the experiments. All authors analyzed the data. AAL and SJ wrote the paper. We would like to thank Leah DeBlander for her assistance with immunohistochemistry, as well as Raj Shah, Erin K. Petruccione, and Jewlyssa Pedregon for their assistance with histology.

II.2. Introduction

The activity of neurons in the auditory cortex of mammals is commonly suppressed by pure tones outside the neurons' receptive fields (Abeles and Goldstein, 1972; Nelken et al., 1994), or sounds of high bandwidth (Rauschecker and Tian, 2004; O'Connor et al., 2010; Li et al., 2019), yet the mechanism by which the auditory system integrates information across many frequency channels to produce these suppressed responses in the cortex is not well understood. Specifically, it is not clear to what extent this suppression is inherited from upstream auditory areas or mediated by cortical circuits. Here, we investigated the role of inhibitory auditory cortical circuits in mediating spectral surround suppression. When classified

according to gene-expression patterns, distinct classes of inhibitory interneurons within a particular cortical region display different physiological responses and anatomical connectivity (Moore et al., 2013; Kvitsiani et al., 2013; Li et al., 2014, 2015; Kuchibhotla et al., 2017; Liang et al., 2019), suggesting a difference in function between these cell types (Adesnik et al., 2012; Natan et al., 2015; Phillips et al., 2017; Kato et al., 2017). To evaluate the contributions of distinct sources of inhibition to cortically mediated surround suppression of evoked responses to high bandwidth sound stimuli, we studied the two most common genetically-defined types of cortical inhibitory interneurons, parvalbumin-expressing (PV^+) and somatostatin-expressing (SOM^+) cells (Rudy et al., 2011). We found that SOM^+ cells play a more dominant role in mediating sustained auditory cortical spectral surround suppression than PV^+ cells, suggesting a dominant mechanistic role of SOM^+ cells in the global integration of auditory stimuli.

II.3. Materials and Methods

II.3.1. Animals

A total of 31 transgenic adult mice of both sexes (4 SOM-Cre, 7 PV-Cre, 16 SOM::ChR2 and 4 PV::ChR2), age 3-7 months, were used in this study. The PV-Cre and SOM-Cre driver lines (008069 and 013044 from JAX) were used in combination with viral transfection, or crossed with LSL-ChR2 mice (012569 from JAX) to produce mice expressing ChR2 in parvalbumin-expressing (PV^+) or somatostatin-expressing (SOM^+) inhibitory interneurons. All procedures were carried out in accordance with National Institutes of Health standards and were approved by the University of Oregon Institutional Animal Care and Use Committee.

II.3.2. Experimental details

II.3.2.1. Auditory stimuli

Electrophysiology was carried out inside single-walled sound-isolation boxes (IAC Acoustics, North Aurora, IL). All auditory stimuli were generated using Python software developed in-house (https://taskontrol.readthedocs.io/) and were delivered from a free-field speaker (MF1 Multi-Field Magnetic Speakers, Tucker-Davis Technologies, Alachua, FL) facing the mouse's ear contralateral to the recording. Mice were head-fixed on top of a freely-moving wheel, leaving them free to move and run while their heads remained stationary.

Recorded cells were tested for their characteristic frequency and peak response to amplitude modulation (AM). Frequency tuning was determined through the presentation of 100 ms pure tones at 16 frequencies (ranging from 2 to 40 kHz) at 55 dB SPL. This sound intensity was selected in order to match the power of the individual frequency components in 70 dB SPL white noise. The preferred frequency was selected by fitting a Gaussian curve to the cell's frequency response curve and selecting the peak as the estimated best frequency. AM responses were determined through presentation of 500 ms of sinusoidally amplitude modulated white noise with a modulation depth of 100% at 5 modulation rates (ranging from 4 to 64 Hz). AM sounds were presented at a peak intensity of 70 dB SPL. The best modulation rate was then selected as the one that gave the greatest sustained firing rate for each cell.

To determine the degree of surround suppression for each cell, we recorded responses to bandpass-filtered white noise centered at the cell's preferred frequency and amplitude modulated at the cell's preferred rate. Stimuli were presented at 7 different bandwidths: 0 (pure tone), 0.25, 0.5, 1, 2, 4 octaves and white noise. The

white noise stimulus had an intensity of 70 dB SPL. All other stimuli were bandpass filtered versions of this white noise stimulus, with the exception of the pure tone stimulus, which was generated separately as a pure sinusoidal wave. This difference in sound generation made it difficult to precisely match the amplitude of the pure tone stimulus to that of the other stimuli, potentially affecting the interpretability of our results. For this reason, we focused our analysis of surround suppression on the responses to bandpass filtered noise. To test for intensity tuning, additional trials were performed with the white noise stimulus at 50 dB SPL. All sound stimuli were 1000 ms long. Cells were selected for analysis of surround suppression if they were frequency tuned ($R^2 > 0.1$ of Gaussian fit) and the estimated preferred frequency was within 0.3 octaves of the center frequency used during the bandpass-filtered white noise stimuli.

II.3.2.2. Surgical implant for head-fixed recordings

Animals were anesthetized with isoflurane through a nose-cone on a stereotaxic apparatus. Mice were surgically implanted with a head-bar to allow for head-fixed recordings. Bilateral craniotomies and durotomies were also performed over the auditory cortex to allow for acute recordings. Craniotomies were centered at 2.8 mm posterior to bregma and 4.4 mm from midline. All animals were monitored and recovered fully before electrophysiological experiments.

II.3.2.3. Viral injections

AAV5.CBA.Flex.ArchT-tdtomato.WPRE.SV40 (Addgene viral prep # 28305-AAV5) (Han et al., 2011) was injected bilaterally into the auditory cortex of PV-Cre and SOM-Cre mice. Two 90 nL injections were done per hemisphere at 2.6 and 3.0

mm posterior to bregma, 4.4 mm from midline, and at a depth of 1.0 mm from pia. The needle was kept at the injection depth for 3 minutes following injection. The virus was given at least 2 weeks to express prior to electrophysiological recordings.

II.3.2.4. Neural recordings

Electrical signals were collected using an RHD2000 acquisition system (Intan Technologies, Los Angeles, CA) and OpenEphys software (www.open-ephys.org), using silicon probe electrodes (A4x2-tet configuration from NeuroNexus, Ann Arbor, MI). Multiple penetrations were made spanning the mediolateral axis of the craniotomy. Probes were covered in fluorescent dye (DiO, DiI, or DiD; Vybrant cell-labeling solution) before each penetration to verify placement at the conclusion of the experiment. During the experiment, the mouse was head-fixed inside the rig and the protective covering over the craniotomy was removed, exposing the brain. The probe was moved into place, such that its shanks were parallel to the midline of the skull. The probe was held in a vertical position and lowered vertically into the cortex until spikes were detected. We recorded at multiple depths on each penetration, with recording sites typically 100-150 μm apart to avoid recording from the same cells twice.

II.3.2.5. Photo-identification of PV^+ and SOM^+ neurons

PV^+ and SOM^+ cells were identified by evaluating neural responses to the first 10 ms of light pulses in PV::ChR2 and SOM::ChR2 mice. Light pulses were 100 ms long with interstimulus interval of 900 ms, but only the onset responses were used for photo-identification to rule out effects from synaptic transmission. Blue light (wavelength 470 nm) was delivered via an optical fiber attached to the silicon probe

electrodes with the tip about 200 μm from the topmost recording sites (fiber diameter 50 μm). Light power was 1.5-2.5 mW at the fiber tip. PV^+ and SOM^+ cells were identified by their significant ($p < 0.001$) increase in firing rate immediately following light presentation. Putative excitatory cells were identified as cells in SOM::ChR2 mice that did not have positive responses to the light pulses and whose spike widths, defined as the time difference between the sodium peak ("peak") and the potassium peak ("trough"), were greater than 0.4 ms. Because the spike shapes of excitatory cells and SOM^+ cells can be very similar, putative excitatory cells were selected only from SOM::ChR2 mice in order to exclude SOM^+ cells by their laser response and exclude PV^+ cells by spike shape. While it is reasonable to expect that this method does not exclude every inhibitory cell, we believe the majority of cells classified as putative excitatory cells are excitatory.

II.3.2.6. Inactivation of PV^+ and SOM^+ neurons

PV^+ and SOM^+ cells were inactivated during sound presentation with 1300 ms light pulses (light onset was 100ms before sound onset, light offset was 200ms after sound offset). Green light (wavelength 520 nm) was delivered via an optical fiber attached to the silicon probe electrodes with the tip about 900 μm from the topmost recording sites (fiber diameter 200 μm). Light power was 5 mW at the fiber tip. Laser was presented for 50% of trials. Laser and non-laser trials were randomly interleaved. Laser-induced changes in baseline firing rate were calculated using the first 50 ms after laser onset.

II.3.2.7. Histology

At the conclusion of the experiment, animals were deeply anesthetized with euthasol and perfused through the heart with 4% paraformaldehyde. Brains were extracted and left in 4% paraformaldehyde for at least 24 hours before slicing. Brains were sliced under phosphate-buffered saline on a vibratome with a slice thickness of 50 μm. Brain slices were imaged with a fluorescent microscope (Axio Imager 2, Carl Zeiss) with a 2.5x objective. To determine the locations of our recordings, we manually registered each histology slice containing dye fluorescence to the corresponding coronal section in the Allen Mouse Common Coordinate Framework (Common Coordinate Framework v.3, © 2015 Allen Institute for Brain Science, Allen Brain Atlas API, available from http://brain-map.org/api/index.html). Recordings were considered for analysis only if they were localized to auditory cortical areas.

II.3.2.8. Immunohistochemistry

Animals were deeply anesthetized with euthasol and perfused through the heart with 4% paraformaldehyde, and the brains were postfixed overnight and cryoprotected in 30% sucrose. Sections 30 μm thick were blocked in 10% donkey serum in phosphate-buffered saline for 1 hour. Sections were then incubated for 24 hours in mouse anti-parvalbumin (1:4000, Millipore MAB1572) or rat anti-somatostatin (1:50, Abcam M09204). The sections were then incubated for 2 hours in donkey anti-mouse (1:800, Thermo Fisher Invitrogen SA5-10166) or donkey anti-rat (1:800, Thermo Fisher Invitrogen SA5-10026). Brain slices were imaged with a fluorescent microscope (Axio Imager 2, Carl Zeiss) with a 10x objective. To quantify

the specificity of expression, cells were identified in separate fluorescent channels and subsequently scored for colocalization.

II.3.3. Data analysis

II.3.3.1. Spike sorting

Spiking activity was detected by applying a low threshold (40-45 μV) to bandpass (300 to 6000 Hz) filtered continuous data. Spiking activity of single units was isolated offline using the automated expectation maximization clustering algorithm Klustakwik (Kadir et al., 2014). Isolated clusters were only included in the analysis if less than 2% of inter-spike intervals were shorter than 2 ms. Clusters with 2-5% of inter-spike intervals shorter than 2 ms were automatically refined by iteratively removing the spike with the largest Mahalanobis distance to the cluster centroid in feature space until the cluster had less than 2% of inter-spike intervals shorter than 2 ms. We also calculated a spike quality index, defined as the ratio between the peak amplitude of the waveform and the average variance, calculated using the channel with the largest amplitude. Cells were only included in the analysis if they had a spike quality index greater than 2.5.

II.3.3.2. Suppression index

To determine the degree to which cells are suppressed by sounds of high bandwidth, we calculated a suppression index (SI) as follows:

$$SI = \frac{R_p - R_w}{R_p}$$

Here, R_p is the cell's peak firing rate and R_w is the cell's firing rate in response to white noise, the highest bandwidth stimulus presented. This suppression index is similar to one previously used to quantify surround suppression in the visual cortex (Adesnik et al., 2012; Ayaz et al., 2013). R_p and R_w were calculated using fits from a subtractive surround model.

II.3.3.3. Facilitation index

To determine the degree to which cell responses increase as the bandwidth of the sound stimulus increases from zero (pure tone), we calculated a facilitation index as follows:

$$FI = \frac{R_p - R_{pt}}{R_p}$$

Here, R_p is the cell's peak firing rate and R_{pt} is the cell's firing rate in response to the pure tone stimulus at the cell's preferred frequency. R_p and R_{pt} were calculated using fits from a subtractive surround model that included responses to pure tones.

II.3.3.4. PT vs. WN index

To determine the degree to which cells exhibited a preference for pure tones (the lowest bandwidth stimulus presented) over white noise (the highest bandwidth stimulus presented), we calculated a pure tone (PT) vs. white noise (WN) index as follows:

$$\frac{R_{pt} - R_w}{R_{pt} + R_w}$$

Here, R_{pt} is the cell's firing rate in response to the pure tone stimulus at the cell's preferred frequency, and R_w is the cell's firing rate in response to the white noise stimulus.

II.3.3.5. Intensity index

To determine the degree to which cells were tuned to different intensities of sound, we calculated an intensity index as follows:

$$II = \frac{R_h - R_l}{R_h + R_l}$$

Here, R_h is the cell's firing rate in response to the high intensity stimulus, and R_l is the cell's firing rate in response to the low intensity stimulus. Intensity indices for each cell were calculated using the responses to the pure tone and white noise stimuli to determine the extent to which surround suppression is explainable by intensity tuning.

II.3.3.6. Subtractive surround model fitting

Neuronal responses were modeled using a subtractive surround model similar to a divisive normalization model previously used to describe surround suppression in the visual cortex (Ayaz et al., 2013). In this model, two Gaussian fields provide input to each cell: a driving field G_d and a suppressive field G_s. The sum of their responses to sound stimuli with bandwidth b are:

$$D(b) = \int_{-b}^{b} G_d(x)dx = \mathrm{erf}\Big(\frac{b}{\sqrt{2}\sigma_d}\Big)$$

$$S(b) = \int_{-b}^{b} G_s(x)dx = \mathrm{erf}\left(\frac{b}{\sqrt{2}\sigma_s}\right)$$

Here, σ_d and σ_s are the extents of the two Gaussian fields. The cell's response to sounds of different bandwidths is then computed as the difference of the two field responses:

$$R(b) = R_0 + R_d D(b) - R_s S(b)$$

Here, R_0 is the spontaneous firing rate, and R_d and R_s are the strengths of the driving and suppressive fields, respectively. The model was fit by minimizing the mean squared error between predicted and observed firing rates. A subtractive surround model was selected to model the responses of auditory cortical neurons because a divisive normalization model was not able to accurately capture the responses of cells that were suppressed below their spontaneous firing rate.

II.3.3.7. Mechanistic model

The feedforward neural model presented in Fig. II.10 consists of an output excitatory neuron that receives three types of inputs: (1) feedforward excitatation from other cells (including thalamic inputs), (2) feedforward inhibition from PV^+ cells, and (3) feedforward inhibition from SOM^+ cells. The response of the output excitatory cell (R) is calculated as the weighted sum of the input $r(x)$ from each frequency channel x, passed through a rectifying non-linearity:

$$R = f\left(\sum_{\phi}\sum_{x} w_\phi(x)\, r(x)\right)$$

$$f(y) = \max(0, y)$$

where the weights $w_\phi(x)$ for each input type $\phi = \{Th, PV, SOM\}$ follow a Gaussian profile defined by two parameters: the maximum strength (A_ϕ) and the breadth of integration across frequency channels (σ_ϕ):

$$w_\phi(x) = A_\phi e^{-\frac{1}{2}\left(x/\sigma_\phi\right)^2}$$

The parameters σ_ϕ effectively combine the response-tuning width of pre-synaptic cells of type ϕ with the range of those cells' synaptic projections to excitatory cortical cells. The input $r(x)$ is simulated as a rectangular function of unit amplitude, centered around location $x = 0$. The width of this function defines the bandwidth of the stimulus. Note that when thinking of $r(x)$ as representing thalamic inputs to the auditory cortex, our model neglects to account for any surround suppression in the thalamus (or more generally, in the excitatory input to excitatory cells).

We constructed a model with 101 frequency channels covering the entire tonotopic axis of the auditory cortex, which in mice covers about six octaves. For the examples in Fig. II.10B,C, the following synaptic strength parameters were used: $A_{PV} = -25$, $A_{SOM} = -25$, $A_{Th} = 100$, $\sigma_{PV} = 0.8$ octaves, $\sigma_{SOM} = 1.6$ octaves, $\sigma_{Th} = 0.4$ octaves. These parameters were selected based on the results of Kato et al. (2017), which found that SOM$^+$ cells have a larger frequency tuning width and larger synaptic projection range than PV$^+$ cells. We chose to base our model on this study over others due to the similarity in experimental techniques, chiefly the use of long duration sound stimuli in awake animals for measuring tuning widths. The additional simulations exploring the parameters space, shown in Fig. II.10D,E, used A_{PV} and A_{SOM} in the range 1-30% of A_{Th}, σ_{Th} in the range 20-100% of σ_{PV}, and σ_{SOM} in the range 100-200% of σ_{PV}, with A_{Th} and σ_{PV} fixed at the values given above.

II.3.3.8. Statistics

To test for statistically significant effects across cells (e.g. comparing SIs across excitatory, PV^+, and SOM^+ cells), we used the non-parametric Wilcoxon rank-sum test, because the data were rarely normally distributed and of equal variance. To test for significant effects within cells (e.g. testing effects of laser inactivation), we used the non-parametric Wilcoxon signed-rank test when testing across two conditions, or the Kruskal-Wallis test when testing across more than two conditions. To test for significant correlations between two continuous variables, we computed a least-squares linear regression. A Bonferroni correction was applied in situations where multiple comparisons were made.

II.4. Results

II.4.1. Inhibitory cells exhibit less spectral surround suppression than excitatory cells

To identify populations of cells involved in global integration, we first evaluated the degree to which distinct cell types exhibit surround suppression. To evaluate the responses of PV^+ and SOM^+ cells, we obtained single-unit extracellular recordings in the auditory cortex (Fig. II.1G) of awake mice expressing the light-gated ion channel channelrhodopsin-2 (ChR2) in either PV^+ cells (Fig. II.1A) or SOM^+ cells (Fig. II.1D). We optogenetically identified PV^+ and SOM^+ cells as those exhibiting positive responses to the first 10 ms of pulses of blue light (Fig. II.1J). Putative excitatory cells were defined as neurons that did not have a significant positive response to laser stimulation and had a spike width greater than 0.4 ms (Fig. II.1I,J). Because cells that do not respond to laser in PV::ChR2 mice could be

SOM$^+$ or excitatory, and the shapes of these cell types largely overlap, we focused our initial analysis on putative excitatory cells from SOM::ChR2 mice, in which excitatory cells are easier to distinguish. To quantify the degree of spectral surround suppression in each cell, we presented sound stimuli of different bandwidths centered on each cell's preferred frequency to the ear contralateral to the recorded hemisphere (Fig. II.2A,B). We then fit the cell's responses using a subtractive surround model (see Methods) and computed a suppression index (SI) defined as the normalized difference between the cell's maximum sound-evoked firing rate and its firing rate in response to white noise, following previous studies exploring a similar effect in the visual system (Adesnik et al., 2012; Ayaz et al., 2013).

Fig. II.2C depicts the responses of a typical putative excitatory cell that displays strong spectral surround suppression. While the sustained responses of this cell to a low bandwidth stimulus at its preferred frequency were large, sound responses decreased with increasing bandwidth even though the power in the preferred frequency remained the same. We found that surround suppressed responses were common in excitatory cells in the auditory cortex, with the population showing a median suppression index of 0.49 (Fig. II.2F). Suppression index was negatively correlated with cortical depth for excitatory cells, showing a median SI of 0.60 for supragranular layers and 0.43 for infragranular layers ($r = -0.259$, $p = 0.006$, linear regression). Excitatory cells in primary auditory areas ($N = 68$) showed similar amounts of suppression to excitatory cells recorded in non-primary auditory areas ($N = 48$; $p = 0.556$, Wilcoxon rank-sum test).

In comparison to excitatory cells, typical PV$^+$ (Fig. II.2D) and SOM$^+$ (Fig. II.2E) cells showed low amounts of surround suppression, as high bandwidth sounds tended to robustly drive these cells above their spontaneous firing rate.

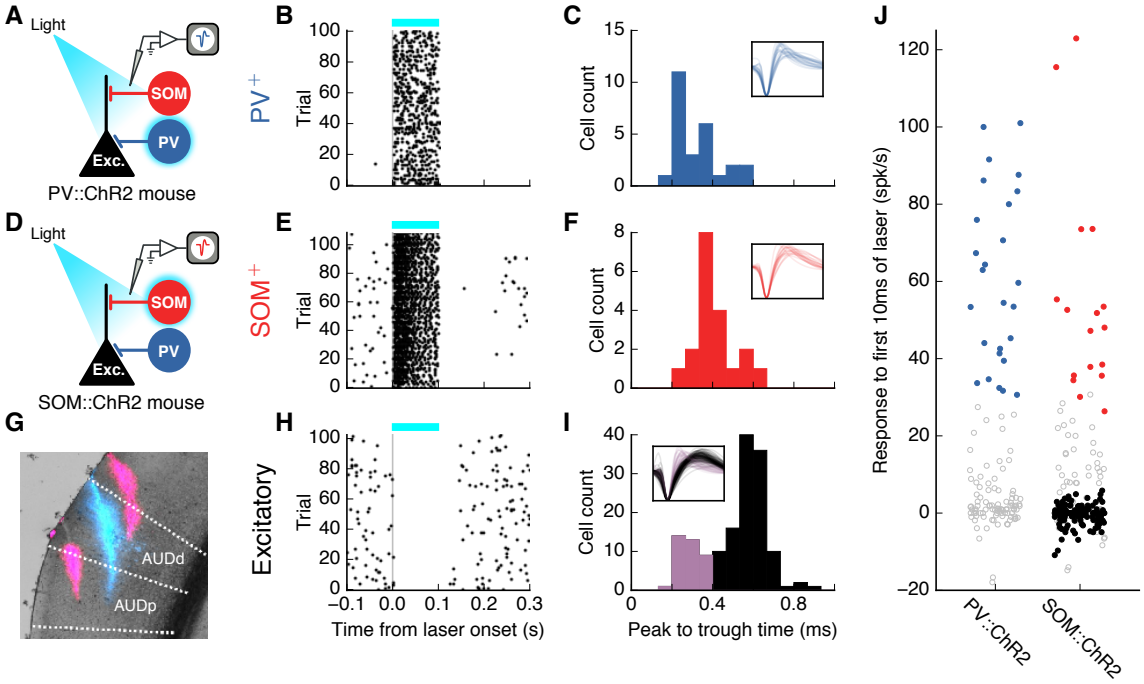

FIGURE II.1. Photoidentification of auditory cortical cell types
(A) Identification of PV$^+$ cells in PV::ChR2 mice by their responses to laser stimulation. **(B)** Response of an example identified PV$^+$ cell to 100 ms pulses of blue laser (blue bar). **(C)** Spike widths of all identified PV$^+$ cells ($N = 26$). Inset: normalized spike waveforms of all identified PV$^+$ cells. Voltage traces are 1.33 ms long. **(D)**, Identification of SOM$^+$ cells in SOM::ChR2 mice by their responses to laser stimulation. **(E)**, Response of an example identified SOM$^+$ cell to 100 ms pulses of blue laser (blue bar). **(F)**, Spike widths of all identified SOM$^+$ cells ($N = 19$). **(G)**, Coronal brain slice (AP: -2.78 mm) showing different electrode tracks: magenta (DiI) and blue (DiD). Recordings were performed at multiple sites along each penetration. AUDp, Primary auditory area; AUDd, dorsal auditory area, according to Allen Mouse Brain Atlas. **(H)**, Response of an example putative excitatory cell to 100 ms pulses of blue laser (blue bar). **(I)**, Spike widths of all cells that did not have positive responses to laser from SOM::ChR2 animals. Black: cells classified as putative excitatory cells ($N = 116$). Purple: cells with narrow spikes (peak to trough < 0.4 ms, $N = 37$) were not classified as putative excitatory cells. **(J)**, Laser-evoked change in firing for all frequency-tuned cells ($N = 122$ from PV::ChR2 mice, 204 from SOM::ChR2 mice) during the first 10 ms of the laser pulse. Identified PV$^+$ cells are highlighted in blue, identified SOM$^+$ cells in red, and putative excitatory cells in black. Cells not falling into any of the above three categories are shown in gray. PV$^+$ and SOM$^+$ cells were identified by their positive, low-latency responses to blue laser ($p < 0.001$, Wilcoxon rank-sum test). Two SOM$^+$ cells with laser-induced firing rates of over 200 Hz are not shown.

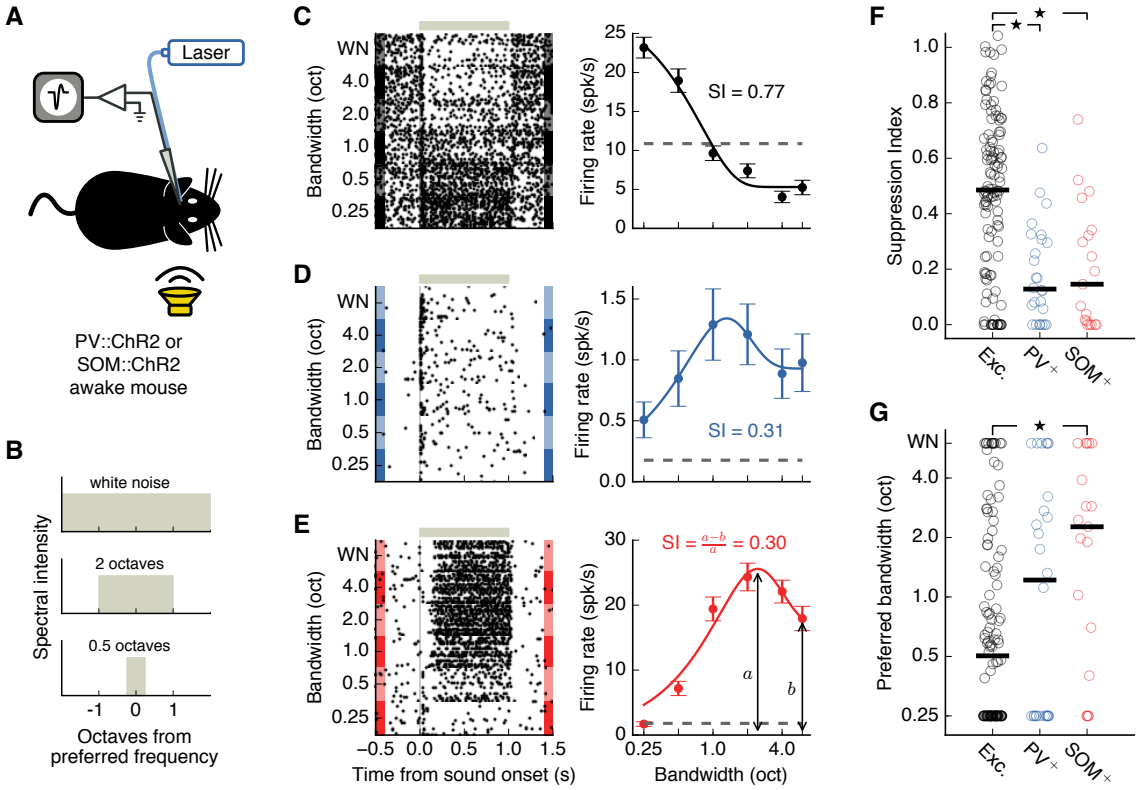

FIGURE II.2. Inhibitory interneurons in AC exhibit less spectral surround suppression than excitatory neurons.
(A), Setup for electrophysiological recordings from the auditory cortex during contralateral sound presentation. **(B)**, Frequency spectra of auditory stimuli used to estimate bandwidth tuning. **(C)**, Left: response of the example putative excitatory cell depicted in Fig. II.1H to amplitude modulated sounds of different bandwidths. Gray bar indicates the sound duration. Right: bandwidth tuning curve of the sustained response (200-1000 ms after sound onset). Dashed line indicates spontaneous firing rate. Error bars are s.e.m. This cell shows a typical surround suppressed response: lower firing for high bandwidth stimuli than for low bandwidth stimuli. **(D)**, Same as **C** for the PV$^+$ cell depicted in Fig. II.1B. **(E)**, Same as **C** for the SOM$^+$ cell depicted in Fig. II.1E. **(F)**, Spectral surround suppression for all recorded putative excitatory ($N = 116$), PV$^+$ ($N = 26$), and SOM$^+$ cells ($N = 19$). Black bars indicate medians. Inhibitory cells were significantly less suppressed than excitatory cells (Exc.-PV$^+$ $p = 5.9 \times 10^{-6}$, Exc.-SOM$^+$ $p = 0.00039$, PV$^+$-SOM$^+$ $p = 0.863$, Wilcoxon rank-sum test). **(G)**, SOM$^+$ cells reach their peak firing rates at significantly higher bandwidths than excitatory cells (Exc.-PV$^+$ $p = 0.327$, Exc.-SOM$^+$ $p = 0.0083$, PV$^+$-SOM$^+$ $p = 0.260$, Wilcoxon rank-sum test). Black bars indicate medians. Stars indicate $p < 0.017$ (alpha value adjusted for multiple comparisons).

Comparing suppression indices across the populations of distinct cell types revealed that both PV^+ and SOM^+ cells exhibited less surround suppression of their sustained sound responses than excitatory cells (Fig. II.2F, Exc.-PV^+ $p = 5.9 \times 10^{-6}$, Exc.-SOM^+ $p = 0.00039$, PV^+-SOM^+ $p = 0.863$, Wilcoxon rank-sum test Bonferroni correction for multiple comparisons). To verify that these differences in surround suppression across cell types could not be explained by our selection of putative excitatory cells only from SOM-ChR2 mice, we performed the same analysis after including cells that did not respond to laser in PV-ChR2 mice, which yielded a comparable magnitude of suppression in excitatory cells ($SI = 0.46$). Differences between excitatory and inhibitory cells were still clearly present when including this additional set of putative excitatory cells (Exc.-PV^+ $p = 0.0003$, Exc.-SOM^+ $p = 0.0056$, PV^+-SOM^+ $p = 0.863$, Wilcoxon rank-sum test). We also found that SOM^+ cells reached their peak response at higher bandwidths compared to putative excitatory cells (Fig. II.2G, Exc.-PV^+ $p = 0.327$, Exc.-SOM^+ $p = 0.0083$, PV^+-SOM^+ $p = 0.260$, Wilcoxon rank-sum test, Bonferroni correction for multiple comparisons).

Our initial characterization of responses to increasing stimulus bandwidth relied on presenting bandpass filtered noise, centered on the cell's preferred frequency, from 0.25 octaves to white noise. We did not include pure tones (sinusoidal waves) in this analysis as these stimuli were generated differently. However, because much work in the field of audition has relied on the presentation of pure tones, we also evaluated what happens when pure tones, which have zero bandwidth, are included in the bandwidth tuning curves and the analysis of surround suppression. We found that all effects described above are present when we include responses to pure tones at each cell's preferred frequency (Fig. II.3). Specifically, excitatory cell responses were

still more strongly suppressed at high bandwidths than the responses of PV^+ and SOM^+ cells (Fig. II.3B, Exc.-PV^+ $p = 1.9 \times 10^{-7}$, Exc.-SOM^+ $p = 5.3 \times 10^{-5}$, PV^+-SOM^+ $p = 0.918$, Wilcoxon rank-sum test, Bonferroni correction for multiple comparisons). Furthermore, a direct comparison between the responses to pure tones and white noise showed that excitatory cells have a higher preference for pure tone stimuli than PV^+ or SOM^+ cells, consistent with their suppression of responses to high bandwidth stimuli (Fig. II.3C, Exc.-PV^+ $p = 0.0088$, Exc.-SOM^+ $p = 0.0026$, PV^+-SOM^+ $p = 0.113$, Wilcoxon rank-sum test, Bonferroni correction for multiple comparisons). Additionally, we still observed that SOM^+ cells prefer significantly higher bandwidths than excitatory cells (Fig. II.3D, Exc.-PV^+ $p = 0.920$, Exc.-SOM^+ $p = 0.0044$, PV^+-SOM^+ $p = 0.056$, Wilcoxon rank-sum test, Bonferroni correction for multiple comparisons). Consistent with their preference for higher bandwidth sounds, we found that the majority of SOM^+ cells preferred white noise to pure tones (Fig. II.3C). The majority of all cells showed some degree of increase in firing rate as bandwidths increased from pure tone, with no significant difference in this facilitation across cell types (Fig. II.3E, Exc.-PV^+ $p = 0.187$, Exc.-SOM^+ $p = 0.498$, PV^+-SOM^+ $p = 0.089$, Wilcoxon rank-sum test, Bonferroni correction for multiple comparisons). These results indicate that the small percentage of cells (10-19% depending on cell type) that respond most strongly to pure tones and more weakly at all nonzero bandwidths do not affect the trends observed in the entire cell population.

Analysis of onset responses (0-50 ms after sound onset) of excitatory cells indicated a much weaker surround suppression during this period compared to that of the sustained responses (median excitatory onset $SI = 0.25$; median excitatory sustained $SI = 0.49$; $p = 0.0001$, Wilcoxon rank-sum test). Differences in surround

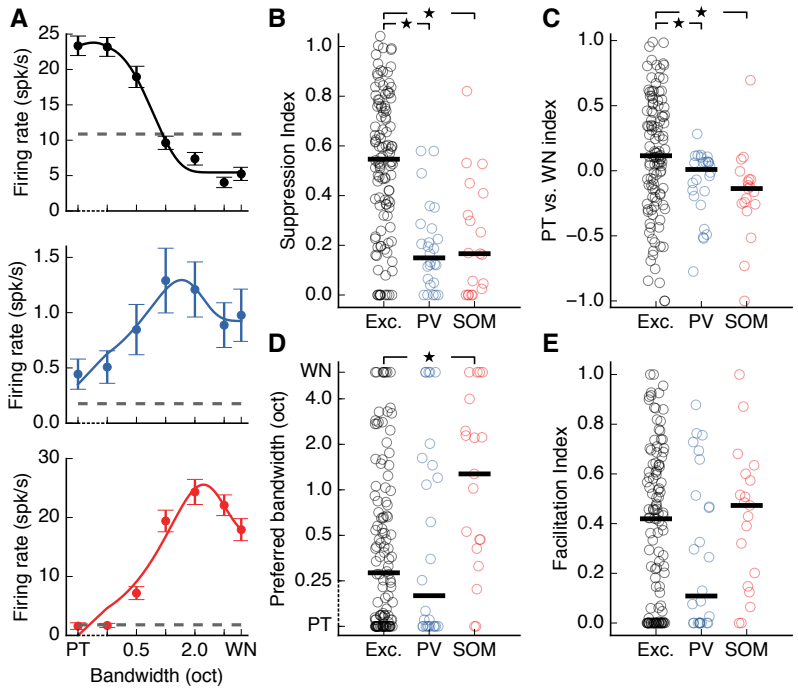

FIGURE II.3. Inclusion of pure tone stimuli in analysis of suppression does not affect results.

(A), Bandwidth tuning curves for the cells depicted in Fig. II.2C,D,E when including responses to pure tones (bandwidth = 0). Our estimation of suppression for these cells is minimally affected by the inclusion of these data points. The dashed axis indicates that data points from 0 (PT) to 0.25 octaves are plotted on a linear scale. **(B)**, Spectral surround suppression for all cells depicted in Fig. II.2F when responses to pure tones are included in the calculation of SI. Inhibitory cells still show significantly less suppression than excitatory cells (Exc.-PV$^+$ $p = 1.9 \times 10^{-7}$, Exc.-SOM$^+$ $p = 5.3 \times 10^{-5}$, PV$^+$-SOM$^+$ $p = 0.918$, Wilcoxon rank-sum test). Black bars indicate medians. **(C)**, When comparing responses to pure tones and white noise, excitatory cells show a significantly higher preference for pure tone stimuli compared to PV$^+$ or SOM$^+$ cells (Exc.-PV$^+$ $p = 0.0088$, Exc.-SOM$^+$ $p = 0.0026$, PV$^+$-SOM$^+$ $p = 0.113$, Wilcoxon rank-sum test). A positive index indicates the cell had a larger response to pure tones than white noise. Black bars indicate medians. **(D)**, The differences in preferred bandwidth seen in Fig. II.2G remain consistent when responses to pure tones are taken into account (Exc.-PV$^+$ $p = 0.920$, Exc.-SOM$^+$ $p = 0.0044$, PV$^+$-SOM$^+$ $p = 0.056$, Wilcoxon rank-sum test). The dashed axis indicates that data points from 0 (PT) to 0.25 octaves are plotted on a linear scale. Black bars indicate medians. **(E)**, There is no significant difference across cell types in facilitation of responses by increasing bandwidth (Exc.-PV$^+$ $p = 0.187$, Exc.-SOM$^+$ $p = 0.498$, PV$^+$-SOM$^+$ $p = 0.089$, Wilcoxon rank-sum test). Black bars indicate medians. Stars indicate $p < 0.017$ (alpha value adjusted for multiple comparisons).

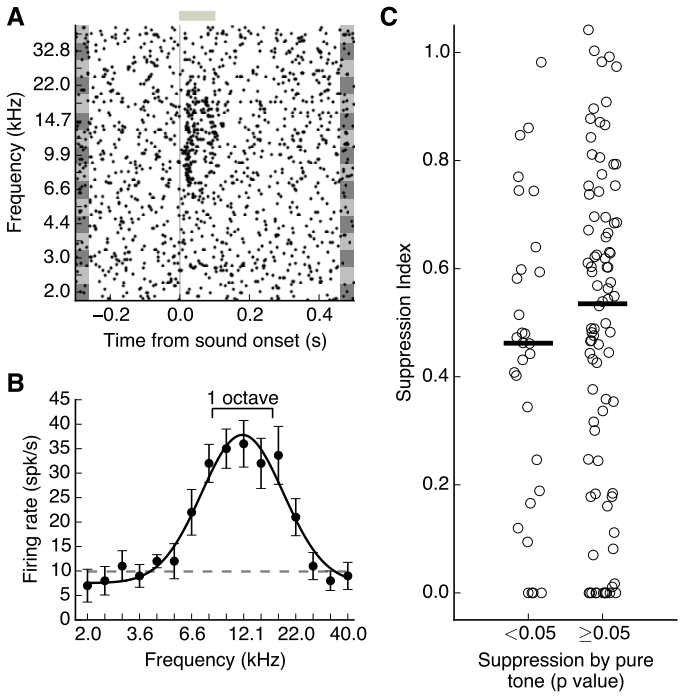

FIGURE II.4. Surround suppression can not be explained by suppression by pure tones.

(A), Response of the putative excitatory cell depicted in Fig. II.2C to pure tones of different frequencies. Grey bar indicates sound duration (100 ms). **(B)**, Frequency tuning curve of cell shown in **A**. Error bars are s.e.m. A Gaussian curve (solid line) was fit to the tuning data, and the cell's preferred frequency was estimated to be the peak of this curve. The dashed line indicates the cell's spontaneous firing rate. The scale bar depicts the range of frequencies in a sound stimulus with a bandwidth of one octave centered on the estimated preferred frequency. Note that although each individual frequency in this range elicits a positive response in this cell, the ensemble of these stimuli leads to a suppressed response (Fig. II.2C). **(C)**, Spectral surround suppression for all recorded putative excitatory cells ($N = 116$), split by whether any pure tone elicited a significant suppression below baseline ($p < 0.05$, Wilcoxon rank-sum test). Black bars indicate medians. Suppression did not significantly differ between the two groups ($p = 0.298$, Wilcoxon rank-sum test).

suppression across some cell types were still present during this period (Exc.-PV^+ $p = 0.025$, Exc.-SOM^+ $p = 0.774$, PV^+-SOM^+ $p = 0.075$, Wilcoxon rank-sum test). Because of the much stronger spectral surround suppression observed during the sustained sound responses of excitatory cells, the remainder of our study focused on the mechanisms responsible for suppression during this period.

The strong sustained suppression brought about by high bandwidth stimuli, such as that observed for the example cell depicted in Fig. II.2C, can occur even when responses to brief pure tone stimuli outside the classical receptive field are only minimally below the spontaneous firing rate (Fig. II.4A,B). Furthermore, suppression of sound responses can be present even for bandwidths encompassing frequencies for which the cell still has strong, positive responses (Fig. II.4A,B). This effect was consistent across the population of putative excitatory cells, and we did not observe any differences in surround suppression between cells that did and did not exhibit significant suppression from pure tone stimuli (Fig. II.4C, $p = 0.298$, Wilcoxon rank-sum test). This implies that the brief pure tone stimuli commonly used to characterize sound responses of auditory cortical neurons are not sufficient to predict the surround suppression observed here.

The observed sustained surround suppression in each cell was not correlated with the cell's preferred frequency (Fig. II.5A). In addition, the observed differences in suppression across cell types cannot be explained by differences in the amplitude modulation rate of the stimulus used in each case (Fig. II.5B). Furthermore, while several putative excitatory cells exhibited sound intensity tuning, sometimes responding more strongly to stimuli of lower intensity, we found that the effects of intensity on evoked responses were independent from the phenomenon of surround suppression (Fig. II.5C). Specifically, while neurons with high suppression indices

were likely to have a preference for low intensity white noise ($r = -0.477$, $p = 9.1 \times 10^{-8}$, linear regression), there was no correlation between suppression index and intensity preference for pure tone stimuli ($r = 0.039$, $p = 0.683$, linear regression), indicating that surround suppression cannot be predicted from intensity preference in the absence of stimuli from the spectral surround.

II.4.2. SOM$^+$ cells exhibit stronger sustained sound-evoked responses than PV$^+$ cells

The lack of strong suppression of responses to high bandwidth stimuli observed in PV$^+$ and SOM$^+$ cells is consistent with these inhibitory cells mediating sustained suppression from the spectral surround. Analysis of the temporal dynamics of PV$^+$ and SOM$^+$ responses revealed that the responses of PV$^+$ cells were stronger at sound onset when compared to responses of SOM$^+$ cells (Fig. II.6B, $p = 0.027$, Wilcoxon rank-sum test). In contrast, SOM$^+$ cells displayed stronger sustained responses than PV$^+$ cells (Fig. II.6C, $p = 0.030$, Wilcoxon rank-sum test). These results imply that SOM$^+$ cells provide greater sustained inhibition in response to sounds of high bandwidth compared to PV$^+$ cells. We hypothesized, therefore, that inhibition from SOM$^+$ cells plays a dominant role in mediating spectral surround suppression in excitatory neurons.

II.4.3. SOM$^+$ inactivation, but not PV$^+$ inactivation, reduces spectral surround suppression in excitatory cells

To test the hypothesis that SOM$^+$ cells contribute more than PV$^+$ cells to surround suppression in excitatory cells, we recorded extracellularly from putative excitatory cells in the auditory cortex of awake mice while optogenetically

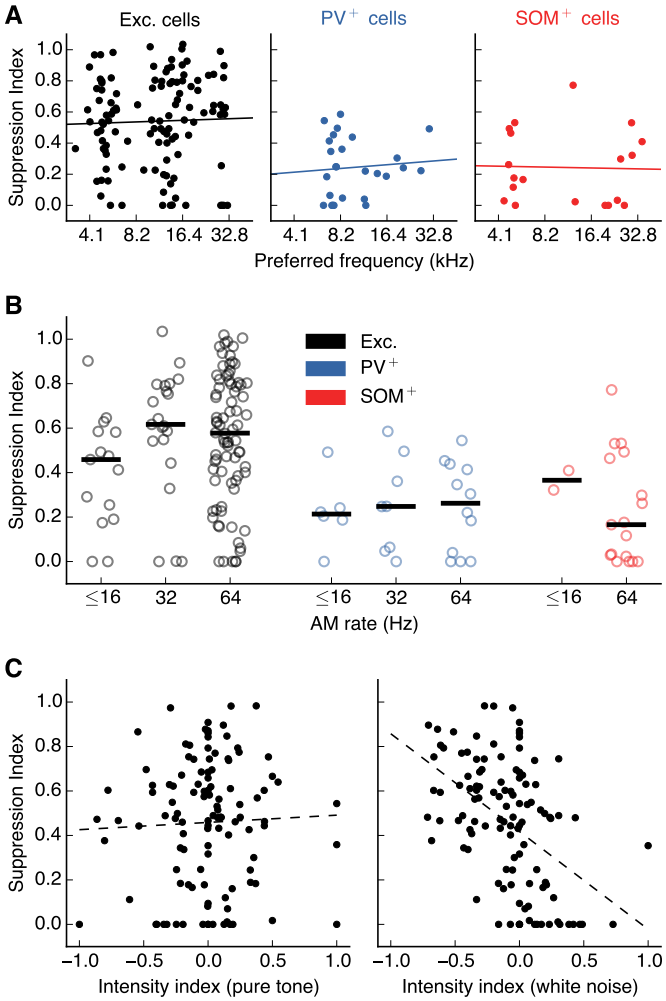

FIGURE II.5. Surround suppression can not be explained by other factors. **(A)**, Suppression index was not correlated with preferred frequency (Excitatory: $r = 0.032$, $p = 0.730$; PV$^+$: $r = 0.085$, $p = 0.681$; SOM$^+$: $r = -0.028$, $p = 0.908$). Lines show linear regressions. **(B)**, Differences in surround suppression across cell types cannot be explained by the stimulus modulation rates used. (Exc. $p = 0.108$, PV$^+$ $p = 0.832$, SOM$^+$ $p = 0.350$, Kruskal-Wallis test for effect of AM rate on SI within each cell type). **(C)**, Left: there was no statistically significant correlation between surround suppression and intensity tuning for pure tones ($r = 0.039$, $p = 0.683$). A negative intensity index means the low intensity pure tone elicited a higher sustained response than the high intensity pure tone. The line shows a linear regression. Right: intensity tuning for white noise is negatively correlated with surround suppression ($r = -0.477$, $p = 9.1 \times 10^{-8}$, linear regression).

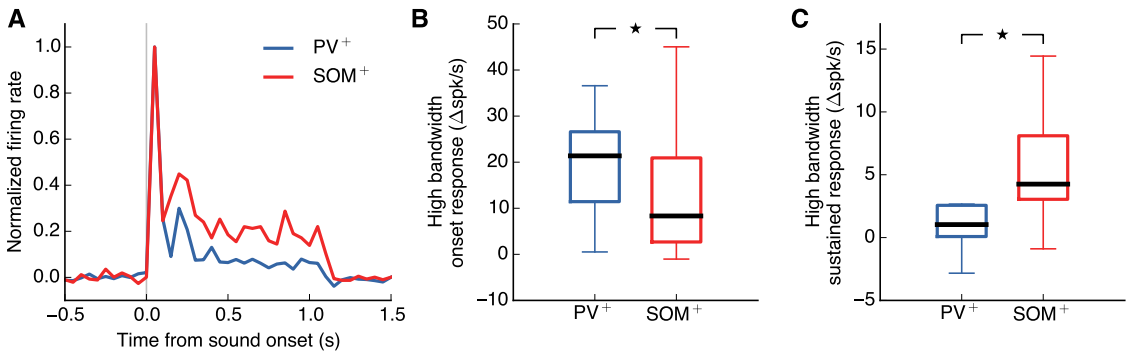

FIGURE II.6. SOM$^+$ cells exhibit stronger sustained responses to high bandwidth stimuli than PV$^+$ cells.
(A), Median response across all PV$^+$ cells (blue) and SOM$^+$ cells (red) included in Fig. II.2 to high bandwidth sound stimuli ($\geq$ 4 octaves), baseline subtracted and normalized so response to sound onset for both cell types is 1. Responses of SOM$^+$ cells do not drop off after onset to the same extent as PV$^+$ cell responses. **(B)**, Onset responses to high bandwidth sound stimuli ($\geq$ 4 octaves) are significantly higher for PV$^+$ cells than SOM$^+$ cells ($p = 0.027$, Wilcoxon rank-sum test). Black bars indicate medians. Boxes extend from the lower to the upper quartile. Whiskers indicate the range. **(C)**, Sustained responses to high bandwidth sound stimuli ($\geq$ 4 octaves) are significantly higher for SOM$^+$ cells than PV$^+$ cells ($p = 0.030$, Wilcoxon rank-sum test). Stars indicate $p < 0.05$.

inactivating either PV^+ cells (Fig. II.7A) or SOM^+ cells (Fig. II.7C) during sound presentation. To express the light-driven outward proton pump ArchT (Han et al., 2011) in these inhibitory cell populations, we injected a Cre-dependent adeno-associated virus (AAV5-Flex-ArchT-tdTomato) in either PV-Cre or SOM-Cre mice. Expression of the virus spanned the majority of the primary auditory area (median range of transfection: -3.45 mm to -2.05 mm posterior from bregma; range of primary auditory area: -3.58 mm to -1.65 mm posterior from bregma). All recordings were performed in transfected areas (median range of recordings: -3.08 mm to -2.35 mm posterior from bregma, see Fig. II.7A,C for examples). Immunohistochemical analysis revealed that, in PV-Cre mice, an anti-PV antibody labeled 84% of transfected cells, and in SOM-Cre mice, an anti-SOM antibody labeled 90% of transfected cells (Fig. II.7B,D). Presentation of the laser rapidly and reliably reduced the responses of a subset of auditory cortical neurons (Fig. II.8A,D). When analyzing the responses of cells showing immediate laser-induced suppression of firing rates, we found that they remained suppressed for the duration of the laser stimulus (Fig. II.8B,E), implying that the laser power used was sufficient to inactivate cells expressing ArchT and overcome any paradoxical network effects that may arise from inactivating inhibitory cells. Moreover, laser presentation had a significantly higher effect on firing rate when directed at the auditory cortex than when directed away (Fig. II.8C,F), indicating that our results can not be solely explained by visual stimulation from the laser.

Fig. II.9A,B depict the sound responses of a typical surround-suppressed putative excitatory cell with and without inactivation of PV^+ cells. Despite the overall increase in sound-evoked firing rate, the cell maintained its previous degree of suppression (control $SI = 0.75$, PV^+ inactivated $SI = 0.79$). In contrast, SOM^+

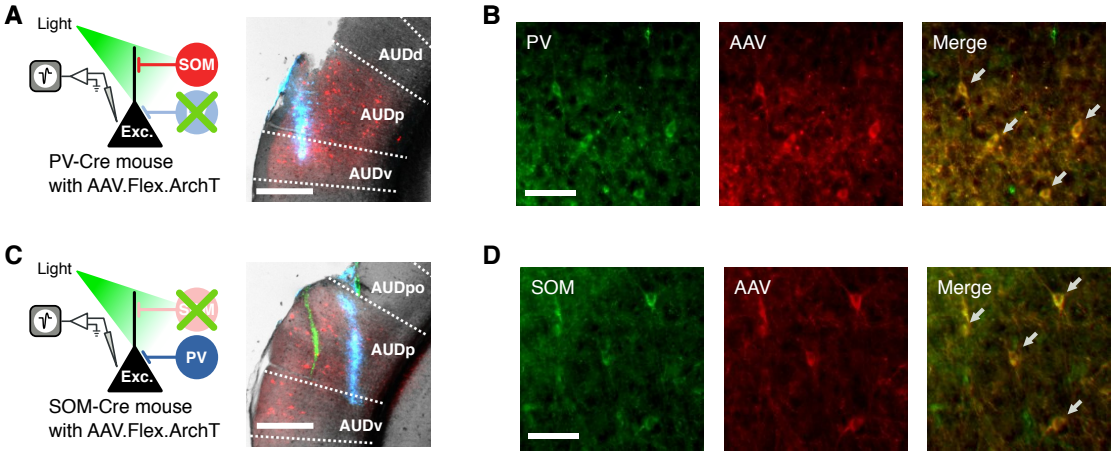

FIGURE II.7. Immunohistochemical verification of viral transfection. **(A)**, Left: Recordings from AC during photo-inactivation of PV^+ cells. Right: Coronal brain slice (AP: -2.35 mm) showing an electrode track (blue, DiD) and the extent of virus expression at the recording location (red, tdTomato) in a PV-Cre mouse. Scale bar is 500 μm. (AUDp: primary, AUDd: dorsal, AUDv: ventral, AUDpo: posterior auditory areas). **(B)**, Confirmation of transfection specificity. Cells labeled with an antibody against PV (left) expressed ArchT-tdTomato (center) as indicated by the arrows (right). Scale bar is 50 μm. **(C)**, Left: Recordings from AC during photo-inactivation of SOM^+ cells. Right: Coronal brain slice (AP: -3.18 mm) showing electrode tracks (blue, DiD; green, DiO) and the extent of virus expression at the recording location (red, tdTomato) in a SOM-Cre mouse. Scale bar is 500 μm. **(D)**, Cells labeled with an antibody against SOM (left) expressed ArchT-tdTomato (center) as indicated by the arrows (right). Scale bar is 50 μm.

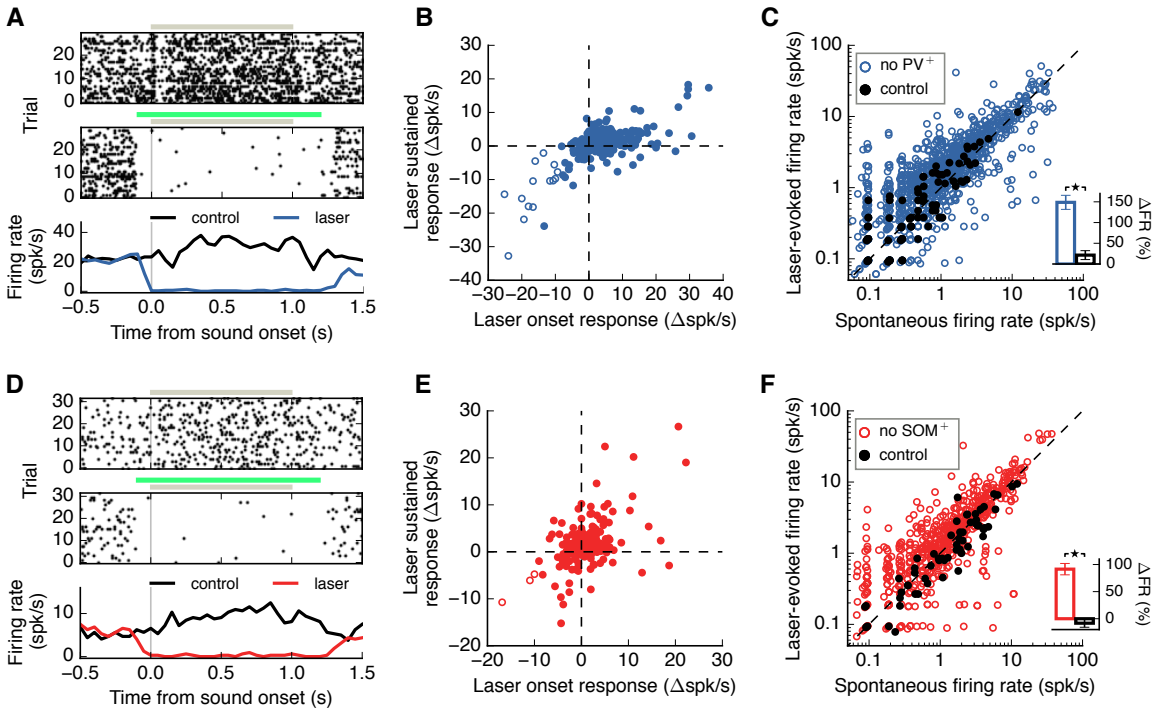

FIGURE II.8. Inactivation of inhibitory cells in the auditory cortex. **(A)**, Response of a cell from a PV-Cre mouse to a 0.25 octave sound stimulus alone (top), or paired with laser (middle). Grey bars indicate sound duration, green bar indicated laser duration. **(B)**, Change in firing rates of all sound-responsive cells from PV-Cre mice ($N = 543$ cells) at laser onset (first 50 ms) *vs.* during sustained laser presentation (300-1100 ms after laser onset). The cells whose responses were significantly suppressed at laser onset (open dots, $N = 16$ cells) remained suppressed for the duration of the laser stimulus. **(C)**, Laser-induced firing rates (50 ms before sound onset) of single units were higher than spontaneous firing rates when laser was directed at the auditory cortex (blue points, $N = 1324$ cells, $p = 2.3 \times 10^{-54}$, Wilcoxon signed-rank test), but not when laser was directed away (black points, $N = 147$ cells, $p = 0.064$, Wilcoxon signed-rank test). Inset: Directing the laser at the auditory cortex led to a stronger change in firing rate compared to the control condition ($p = 3.5 \times 10^{-8}$, Wilcoxon rank-sum test). Error bars are s.e.m. **(D)**, Same as **A** for an example cell from a SOM-Cre mouse. **(E)**, Same as **B**, but for all sound-responsive cells from SOM-Cre mice ($N = 373$). Cells showing significant suppression at laser onset (open dots, $N = 3$) remained suppressed for the duration of the laser stimulus. **(F)**, Same as **C** for SOM-Cre mice. Laser-induced firing rates were higher than spontaneous firing rates when laser was directed at the auditory cortex (red points, $N = 809$ cells, $p = 1.0 \times 10^{-30}$, Wilcoxon signed-rank test), but lower in the control condition (black points, $N = 78$ cells, $p = 0.015$, Wilcoxon signed-rank test). Inset: Directing the laser at the auditory cortex led to a stronger change in firing rate compared to the control condition ($p = 3.9 \times 10^{-9}$, Wilcoxon rank-sum test).

inactivation led to a reduction in the degree of suppression in another typical putative excitatory cell (Fig. II.9C,D, control $SI = 0.84$, SOM^+ inactivated $SI = 0.07$). In our sample of putative excitatory neurons, we found that SOM^+ inactivation led to a statistically significant reduction in sustained suppression (20% reduction on average), while PV^+ inactivation led to a small reduction (7.6% on average) that did not reach statistical significance (Fig. II.9E, SOM^+ inactivation $p = 0.0013$, PV^+ inactivation $p = 0.057$, Wilcoxon signed-rank test). To ensure that the observed reduction in suppression was not a result of the larger sample of excitatory neurons measured during SOM^+ inactivation, we quantified the same effect after downsampling our SOM^+ inactivation data to match the sample size of the PV^+ inactivation data. Running this analysis 1000 times yielded a statistically significant effect when inactivating SOM^+ cells 99.5% of the time, supporting the validity of the result. These results remained consistent when responses to pure tone stimuli were included in our estimation of surround suppression during inhibitory cell inactivation (SOM^+ inactivation $p = 0.00032$, PV^+ inactivation $p = 0.248$, Wilcoxon signed-rank test). Analysis of onset responses also showed that neither PV^+ nor SOM^+ inactivation had any significant effect on suppression of onset sound responses (PV^+ inactivation $p = 0.304$, SOM^+ inactivation $p = 0.339$, Wilcoxon signed-rank test). Furthermore, the effect of PV^+ and SOM^+ inactivation on suppression was not correlated with cortical depth (PV^+ inactivation: $r = 0.080$, $p = 0.696$; SOM^+ inactivation: $r = 0.217$, $p = 0.178$; linear regression).

We then tested whether the observed reduction in surround suppression due to SOM^+ inactivation was the result of a decrease in peak response, or an increase in the response to high bandwidth stimuli (white noise), as only the latter would imply that SOM^+ cells provide information about the surround. We found that

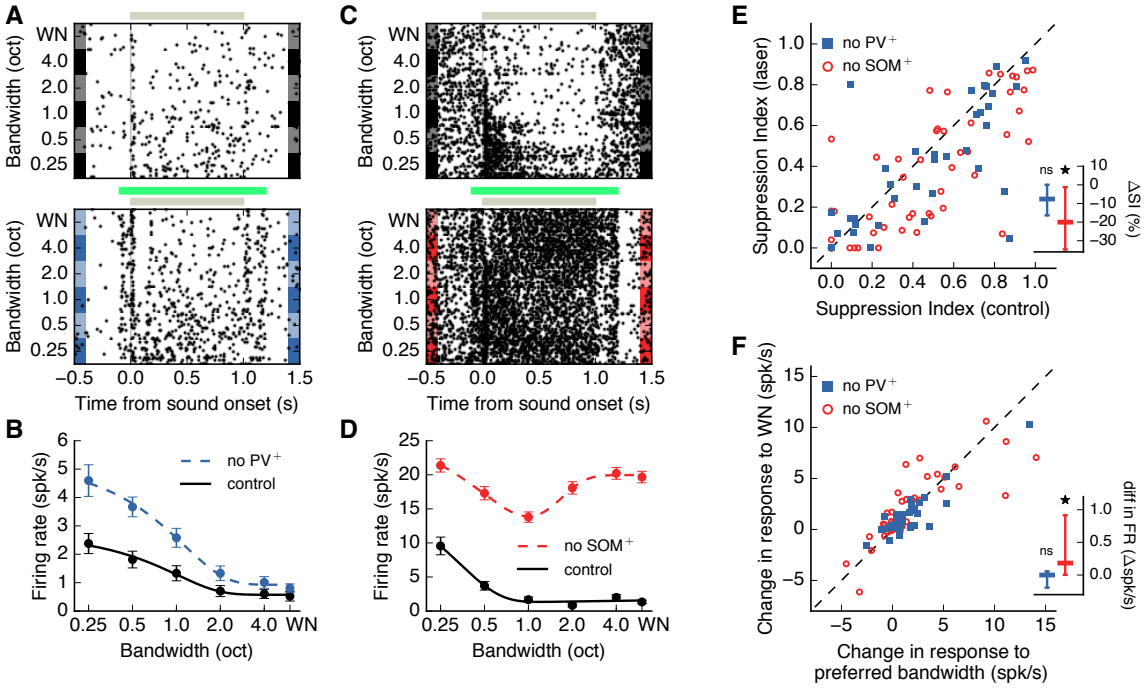

FIGURE II.9. SOM$^+$ cells contribute to spectral surround suppression to a greater extent than PV$^+$ cells.

(A), Responses of an example putative excitatory cell to sounds of different bandwidths in the control condition (top) or during PV$^+$ inactivation (bottom). Gray bar indicates sound duration, green bar indicates laser duration. **(B)**, Bandwidth tuning curve of sustained responses of example cell from **A**. Error bars are s.e.m. PV$^+$ inactivation results in a negligible change in suppression (control $SI = 0.75$, PV$^+$ inactivated $SI = 0.79$). **(C), (D)**, Same as **A, B** for a different putative excitatory cell during SOM$^+$ inactivation, which results in a large change in suppression due to increased responses to high bandwidth stimuli (control $SI = 0.84$, SOM$^+$ inactivated $SI = 0.07$). **(E)**, Inactivation of SOM$^+$ cells significantly reduces surround suppression in excitatory cells ($N = 51$ cells, $p = 0.0013$, Wilcoxon signed-rank test), while inactivation of PV$^+$ cells does not ($N = 40$ cells, $p = 0.057$, Wilcoxon signed-rank test). Inset: percent change in suppression evoked by laser (laser SI − control SI). Star indicates $p < 0.05$. **(F)**, Firing rate for high bandwidth stimuli (white noise) increases more than firing rate for stimuli of the preferred bandwidth during SOM$^+$ inactivation ($p = 0.015$, Wilcoxon signed-rank test). The effects of PV$^+$ inactivation do not significantly differ by bandwidth ($p = 0.427$, Wilcoxon signed-rank test). Four points above the dashed line from SOM$^+$ inactivation are outside the plot range. Inset: difference in change in firing rate evoked by laser between the white noise and preferred bandwidth conditions. A positive difference indicates a larger effect during the white noise condition. Star indicates $p < 0.05$.

during SOM^+ inactivation the response to white noise increased more than the response to the cell's preferred bandwidth, resulting in a reduction in surround suppression (Fig. II.9F, no SOM^+ $p = 0.015$, Wilcoxon signed-rank test). In contrast, the effect of PV^+ inactivation did not differ by bandwidth ($p = 0.427$, Wilcoxon signed-rank test). These results indicate that SOM^+ cells mediate global integration of frequency information by inhibiting excitatory neural responses when spectrally distant frequencies of sounds are present.

II.4.4. Differences in spectral integration among cell classes accounts for their distinct roles in surround suppression

To systematically explore which features of the inputs received by excitatory cells account for the surround suppression observed in our experiments, we developed a simple, proof-of-concept model for the response tuning of excitatory cortical neurons. We modeled the response tuning of excitatory neurons given the tuning of the various inputs they receive, while ignoring several features of cortical circuitry, such as recurrent cortical and thalamocortical interactions, and spectral surround suppression in the feedforward thalamic input to the cortex. Specifically, we simulated the responses of a cortical excitatory model neuron which receives three types of inputs: (1) excitation from other cells (including thalamic inputs), (2) inhibition from PV^+ cells, and (3) inhibition from SOM^+ cells (Fig. II.10A). Results from awake mice have shown that SOM^+ cells have broader frequency tuning than PV^+ or excitatory cells (Kato et al., 2017). These results suggests that SOM^+ cells integrate information across a wider range of frequency channels than PV^+ or excitatory cells, consistent with our findings when we characterized bandwidth tuning in these cell types (Fig. II.2G). Given the observed differences in tuning

among inhibitory cell types, we set the width of the kernel of integration for SOM^+ inhibition (σ_{SOM}) to be twice as large as that of PV^+ inhibition (σ_{PV}), and tested if this feature was sufficient to account for the differential roles in spectral surround suppression played by these cell types.

In response to stimuli of different bandwidths, this simple model replicated the observed spectral surround suppression observed in the auditory cortex (Fig. II.10B black line). To model our inactivation experiments, we eliminated the input from each inhibitory cell class while keeping all other inputs unperturbed. The results from this simulated inactivation of inhibitory cell classes captured the main observations of our experiments in which PV^+ inactivation yields an increase in activity but no major change in spectral surround suppression (Fig. II.10B), while SOM^+ inactivation yields a major change in surround suppression (Fig. II.10C).

To further test whether the effects observed in our simulations were the result of differences in spectral integration between input types and not the values chosen for other model parameters, we simulated multiple neurons, changing parameters such as the breadth of excitation and the maximum strength of each input type, but keeping the breadth of inhibition from SOM^+ cells to be larger than from PV^+ cells. These simulations showed that the effect of inactivating SOM^+ cells on surround suppression is consistently larger than the effect of inactivating PV^+ cells, as measured by changes in suppression index (Fig. II.10D). Moreover, the model accounted for the observation that changes in responses to white noise during SOM^+ inactivation are much larger than changes in responses at the preferred bandwidth, an effect not observed during PV^+ inactivation (Fig. II.10E). These simulations suggest that differences in spectral integration between PV^+ and SOM^+ cells can account for their distinct roles in surround suppression.

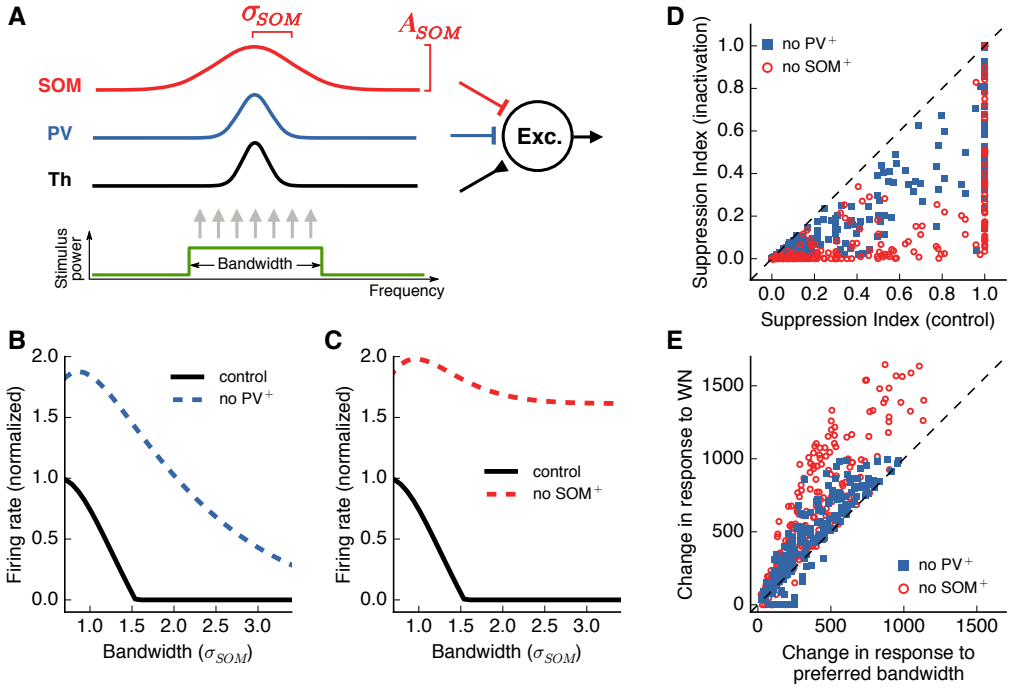

FIGURE II.10. A feedforward model accounts for the distinct roles played by inhibitory cell types in surround suppression.
(A), A simulated output excitatory neuron receives three types of inputs weighted by Gaussian profiles. Integration across frequency channels for the SOM$^+$ input is twice as wide as the integration for PV$^+$ input. **(B)**, Responses of the output neuron for stimuli of different bandwidths. Inactivation of PV$^+$ input results in an increase in responses without major changes in surround suppression. **(C)**, Inactivation of SOM$^+$ input results in a large decrease in surround suppression. **(D)**, Suppression index for each simulated output neuron, with and without inactivation of inhibitory inputs. Change in SI is consistently larger for SOM$^+$ inactivation. **(E)**, Change in response to preferred bandwidth and to white noise stimuli, with and without inactivation of inhibitory inputs (values expressed in arbitrary model response units). The change in response to white noise stimuli is consistently larger than the change for preferred bandwidth during SOM$^+$ inactivation, but not PV$^+$ inactivation.

II.5. Discussion

In this study, we investigated how different sources of cortical inhibition contribute to spectral surround suppression, and by extension, which cortical circuits facilitate global integration over a large range of sound frequencies. By comparing the responses of PV^+ and SOM^+ cells to long broadband sound stimuli, we found that SOM^+ cells maintain high rates of sustained activity, while PV^+ cells instead have strong responses locked to the sound onset. Consistent with previous studies (Blackwell and Geffen, 2017; Liang et al., 2019), these results suggest that PV^+ cells provide fast, transient inhibition, while SOM^+ cells provide sustained inhibition. Combined with the small surround suppression observed in these inhibitory cells, our results imply that SOM^+ cells provide constant information to excitatory cells about the presence of frequencies in their surround. While PV^+ cells display the same lack of suppression seen in SOM^+ cells, only inactivation of SOM^+ cells influenced sustained surround suppression, consistent with the temporal dynamics of their evoked responses. Inactivation of PV^+ cells led to a small and not statistically significant reduction in suppression. This suggests that though PV^+ cells do participate in the general suppression of sound responses, their contribution to the phenomenon of surround suppression at large bandwidths is comparatively small, possibly as a result of their low sustained firing rates. While both PV^+ and SOM^+ cells had relatively high firing rates at sound onset, neither was found to contribute significantly to the suppression of onset sound responses in excitatory cells, suggesting that this effect may not be mediated by cortical inhibition, but rather inherited from upstream auditory areas.

In our characterization of surround suppression across cell types, the majority of PV^+ and SOM^+ cells showed small amounts of suppression in their responses

to high bandwidth stimuli. Despite these responses in inhibitory neurons, many excitatory cells exhibited a monotonic decrease in firing rate as the bandwidth of the sound stimulus increased past their preferred bandwidth. While our inactivation experiments showed that spectral surround suppression is primarily mediated by inhibition from SOM^+ cells, they do not fully explain the relationship between the activity we observe in excitatory and SOM^+ cells. The lack of reduced suppression in excitatory responses at high bandwidths, despite the reduction in inhibitory cell activity, could be explained by complex effects resulting from the recurrence of the cortical network, or by excitatory neurons having reached their lowest level of firing at which small changes in inhibition have little influence. Further study is needed to evaluate these hypotheses.

II.5.1. A model for the response tuning of auditory cortical neurons

To explore the characteristics of SOM^+ cells that explain their dominant role in producing surround suppressed responses to sound, we created a simple feedforward model of excitatory cell responses based on the frequency tuning of the excitatory and inhibitory inputs onto these cells. There exists conflicting information about the tuning properties of excitatory, PV^+, and SOM^+ cells from the auditory cortex, with some studies finding wider tuning in PV^+ cells than excitatory and SOM^+ cells (Li et al., 2015; Liang et al., 2019), others finding similar tuning in PV^+ cells and excitatory cells (Moore et al., 2013), and others finding broader tuning in SOM^+ cells compared to other cell types (Kato et al., 2017). Though the latter study used calcium imaging as opposed to electrophsyiology, their use of awake animals and long duration sound stimuli made their experimental conditions most similar to ours. We therefore chose to base our model parameters on their findings. While our choice of kernel widths

for PV^+ and SOM^+ cells may seem to differ from experimentally derived connection patterns, which show that the spatial extents of the connections between excitatory and inhibitory cells are roughly equal for all cell types (Levy and Reyes, 2012), our kernels represent a combination of the tuning width of presynaptic responses and connection ranges. As such, the broad frequency tuning observed in SOM^+ cells is sufficient to justify our choice of kernels. Furthermore, studies show that SOM^+ cells influence excitatory cell activity at a longer range than PV^+ cells (Li et al., 2014; Kato et al., 2017), providing another possible explanation for the inhibition by spectrally distant stimuli provided by SOM^+ cells. Despite the simplicity of our model, the broad tuning of inhibition from SOM^+ cells was sufficient to explain the effects on surround suppression we found when inactivating SOM^+ cells, consistent with network simulations showing that lateral inhibition can arise from broadly tuned inhibition (Levy and Reyes, 2011). However, this simple model does not fully account for other phenomena present in our data, such as the surround suppression (albeit small) observed in inhibitory cell responses, or the fact that a subset of cells become more surround suppressed with the removal of inhibitory inputs, leaving open an opportunity for future improvements. The inclusion of recurrent interactions across cells, surround suppression of feedforward thalamic inputs, and saturation of inhibitory inputs in the model could potentially address these shortcomings.

II.5.2. A role for SOM^+ cells in mediating lateral inhibition in the sensory cortex

Our results indicate that SOM^+ cells play a dominant role in mediating spectral surround suppression of sustained sound responses by providing excitatory cells with information about their surround. This shows that SOM^+ cells play a role

in modulating auditory cortical activity based on the spectral content of sounds, similar to previous findings showing that SOM^+ cells modulate sound responses depending on temporal context (Natan et al., 2017). Consistent with our findings, inhibition from SOM^+ cells has been shown to mediate long-range lateral inhibition evoked by pure tone stimuli by suppressing excitatory and inhibitory synaptic inputs onto layer 2/3 cells (Kato et al., 2017). However, we found that cells may exhibit surround suppression even when they are not suppressed below baseline by isolated pure tones outside their receptive fields, providing evidence of the non-linearity in the interactions between a cell's response to stimuli within and outside its receptive field.

The phenomenon of surround suppression is also present in sensory systems other than the auditory system. In the visual cortex, responses to visual stimuli of most excitatory cells in layer 2/3 decrease as the stimulus grows in size. This suppression was found to be mediated by inhibition from SOM^+ cells (Adesnik et al., 2012), consistent with our results from the auditory cortex. However, our study found that the strength of sustained responses and degree of suppression seen in PV^+ cells in the auditory cortex do not fully match those found in the visual cortex. These observations suggest that while the role of each cell type may not be fully replicated throughout the cortex, inhibition from SOM^+ cells is a common mechanism for producing responses that are suppressed by the sensory surround.

While our results show that the broad category of SOM^+ cells plays a role in spectral surround suppression, SOM^+ cells can be further classified into distinct subtypes by their anatomy and gene expression patterns (Ma et al., 2006). Recent work in the somatosensory system demonstrated that two different subsets of SOM^+ cells, Martinotti and non-Martinotti, specifically and reciprocally interconnect with

excitatory cells in different cortical layers (Naka et al., 2019), and as such may contribute differently to surround suppression. While the specific contributions of each cell type have yet to be determined, our results demonstrate that these types of SOM^+ cells, either individually or in tandem, are key in shaping the responses of surround suppressed auditory cortical excitatory cells.

II.6. Link to Chapter III

In this chapter, I investigated the cortical mechanisms underlying spectral surround suppression, and identified SOM^+ cells as the cell type responsible for mediating suppression of responses to broadband noise. However, the behavioral relevance of this cortical mechanism is not clear. I hypothesize that responses such as these may be integral in an animal's ability to detect auditory signals by suppressing responses to environmental noise. In Chapter III, I investigate the roles of PV^+ and SOM^+ cells in mediating signal detection to determine if the cell types that contribute most to surround suppression are also most important in identifying the presence of relevant signals against a background of noise.

CHAPTER III

CONTRIBUTIONS OF DISTINCT AUDITORY CORTICAL INHIBITORY NEURON TYPES TO THE DETECTION OF SOUNDS IN BACKGROUND NOISE

III.1. Author contributions

In preparation for publication as: A.A. Lakunina, N. Menashe, S. Jaramillo (2021). Contributions of distinct auditory cortical inhibitory neuron types to the detection of sounds in background noise. AAL and SJ conceived the project and designed the experiments. AAL and NM conducted the experiments. AAL and SJ analyzed the data. AAL and SJ wrote the paper.

III.2. Introduction

The ability to separate background noise from relevant acoustic signals is essential for appropriate sound-driven behavior in natural environments. There is clear evidence that such a separation occurs in the auditory system, where the neural representation of behaviorally relevant stimuli (*e.g.,* intraspecies vocalizations) becomes increasingly noise-invariant along the ascending auditory pathway (Rabinowitz et al., 2013; Schneider and Woolley, 2013; Carruthers et al., 2015). A potential strategy used by the auditory system to separate signals from noise is to emphasize acoustic features that are common in behaviorally relevant stimuli while suppressing features characteristic of background noise. For instance, the auditory system can make use of the statistics of environmental noise, which tends to be broadband and comodulated, to filter it out (Nelken et al., 1999). In this

study, we examined the contribution of cortical inhibition to the implementation of such computation.

The sound-evoked response of a large subset of auditory cortical neurons is suppressed as the bandwidth of the stimulus increases (Rauschecker and Tian, 2004; O'Connor et al., 2010; Li et al., 2019). This phenomenon of spectral surround suppression is in part mediated by cortical inhibition (Lakunina et al., 2020) and provides a plausible mechanism for filtering broadband noise out of auditory stimuli. Distinct classes of cortical inhibitory interneurons are known to have different functions within the sensory cortex (Adesnik et al., 2012; Natan et al., 2015; Phillips et al., 2017). In particular, somatostatin-expressing interneurons (SOM^+) appear to play a unique role in mediating lateral inhibition (Kato et al., 2017) and suppressing neural responses to noise-like broadband stimuli (Lakunina et al., 2020), suggesting a unique role for these cells in filtering background noise. In this study, we sought to determine which sources of cortical inhibition are important for acoustic signal detection in noise, and hypothesized that SOM^+ cells provide a larger contribution than parvalbumin-expressing (PV^+) inhibitory interneurons to the suppression of acoustic environmental noise. We found that inactivation of the auditory cortex resulted in a substantial decrease in the animals' ability to detect auditory signals in noise, confirming a role for auditory cortical circuits in this detection task. However, contrary to our original hypothesis, perturbation of PV^+ or SOM^+ cells separately resulted in similar deficits in signal detection in noise, suggesting that a disrupting of the cortical network dynamics by either cell type is sufficient to impair the ability of the auditory cortex to separate acoustic signals from noise.

III.3. Materials and Methods

III.3.1. Animal subjects

A total of 72 transgenic adult mice of both sexes, age 3-9 months, were used in this study, with 31 mice undergoing surgery for implantation of optical fibers (8 PV::ChR2, 13 PV::ArchT, 10 SOM::ArchT). The PV-Cre and SOM-Cre driver lines (008069 and 013044 from JAX) were crossed with LSL-ChR2 mice (012569 from JAX) or LSL-ArchT mice (021188 from JAX, Han et al. (2011)) to produce mice expressing channelrhodopsin-2 (ChR2) or archaerhodopsin (ArchT) in parvalbumin-expressing (PV^+) or somatostatin-expressing (SOM^+) inhibitory interneurons. All mice were housed in groups of same-sex littermates, and continued to be housed together after surgery whenever possible. Mice were housed in a 12:12 hour light-dark cycle, and all experiments were carried out during the dark period, when the mice were active. All procedures were carried out in accordance with National Institutes of Health Standards and were approved by the University of Oregon Institutional Animal Care and Use Committee.

III.3.2. Behavioral task

The signal detection task was carried out inside single-walled sound-isolation boxes (IAC-Acoustics). Mice were water-restricted to motivate them to perform the task. Free water was provided on days with no experimental sessions. Behavioral data was collected using the taskontrol platform (www.github.com/sjara/taskontrol) developed in our laboratory using the Python programming language (www.python.org). Mice initiated each trial by poking their noses into the center port of a three-port behavior chamber. After a silent delay of

random duration (200–400 ms, uniformly distributed), a sound was presented until the animal withdrew from the port, to a maximum of 500 ms. Animals were required to then choose one of the two side ports to obtain a reward (2 μl of water). 20 mice were trained to report the presence of a tone by going right and the absence of a tone by going left, while 11 mice were trained to report the presence of a tone by going left and the absence of a tone by going right. At the end of the sound stimulus, the mice had 4 seconds to make their choice and go to one of the reward ports. If the mice did not respond in this period of time, the trial was aborted and not considered during data analysis.

Sound stimuli consisted of a bandpass-filtered white noise stimulus acting as a masker and an 8 kHz pure tone stimulus acting as the signal to be detected. The masker was sinusoidally amplitude-modulated at a rate of 8 Hz and depth of 100%, while the pure tone was unmodulated. A pure tone stimulus was present in 50% of trials to ensure mice could not achieve above-chance performance by being biased to one side. The signal-to-noise ratio (SNR) was varied by changing the amplitude of the signal. When the pure tone was present, it was presented simultaneously with the noise, turning on and off at the same time. Within a behavioral session, we used 2 distinct bandwidths (0.25 octaves and white noise) for the masker noise and 3 distinct SNRs (10, 15, 20 dB) for the pure tone signal. The intensity of all frequency components of the noise was a single value that varied on a per-trial basis from 30 to 40 dB-SPL during the initial training, but was fixed for all trials at 40 dB-SPL during testing. Each behavioral session lasted 60-90 min.

III.3.3. Optogenetic stimulation in awake mice

Optical fibers (CFML12U-20, 200 μm core diameter, ThorLabs) were cleaved and etched with hydrofluoric acid for 40 min to obtain a cone-shaped tip. Each optical fiber was glued to a metal guide tube that helped secure the fiber ferrule to the skull. Before implantation, optical fibers were connected to a laser (445 nm for activating ChR2 or 520 nm for activating ArchT) built in-house and the light output calibrated using a PM100D power meter (ThorLabs). To implant the fibers, animals were anesthetized with isoflurane through a nose-cone on a stereotaxic apparatus, then the optical fibers were implanted bilaterally in the auditory cortex (2.8 mm posterior to bregma, 4.4 mm from midline, and 0.5 mm from brain surface). All animals were monitored and recovered fully before returning to water restriction. Fiber locations were verified histologically postmortem.

During a behavioral session, the laser was connected to the implanted optical fibers with flexible fiber optic patch cables (MFP_200/240/900-0.22_2m_FC-MF1.25, Doric Lenses). The cables did not impede the mouse's movement, and 2-4 sessions were done prior to the experimental sessions to acclimate the mouse to the fibers and ensure it could still perform the task. The laser power used was 3 mW at the tip for PV::ChR2 animals and 10 mW at the tip for PV::ArchT and SOM::ArchT animals. These powers have previously been shown to limit illumination to the auditory cortex, driving activity within the auditory cortex, while limiting effects on firing rate in other cortical areas (Weible et al., 2014a,b). Laser was presented in 25% of trials. The laser turned on at sound onset and turned off 100ms after the sound ended or when the mouse entered one of the reward ports, whichever came first. Additional sessions were performed with the patch cables attached to the implant,

but not connected to the optical fibers, to control for any visual effects the laser might have on behavior.

III.3.4. Neural recordings

PV::ArchT mice were surgically implanted with a head-bar to allow for head-fixed extracellular recordings. Bilateral craniotomies (centered at 2.8 mm posterior to bregma and 4.4 mm from midline) were performed to allow for acute recordings from the auditory cortex. All animals were monitored and recovered fully before electrophysiological experiments.

Electrical signals were collected using an RHD2000 acquisition system (Intan Technologies, Los Angeles, CA) and OpenEphys software (www.open-ephys.org), using silicon probe electrodes (A4x2-tet configuration from NeuroNexus, Ann Arbor, MI). During the experiment, the awake mouse was head-fixed and the probe was lowered vertically into the auditory cortex until spikes were detected. We recorded at multiple depths on each penetration, with recording sites typically 100-150 μm apart to avoid recording from the same cells twice.

Cortical PV^+ cells were inactivated during the presentation of 1000 ms sounds with 1300 ms light pulses (light onset was 100 ms before sound onset, light offset was 200 ms after sound offset). Green light (520 nm wavelength) was delivered via an optical fiber (200 μm diameter) attached to the silicon probe electrodes with the tip about 900 μm from the topmost recording sites. Light power was 5 mW at the fiber tip and was presented for 50% of trials, with laser and non-laser trials randomly interleaved.

Spiking activity was detected by applying a low threshold (40-45 μV) to the bandpass-filtered signals (300 to 6000 Hz). Spiking activity of single units was

isolated offline using the automated expectation maximization clustering algorithm Klustakwik (Kadir et al., 2014). Isolated clusters were only included in the analysis if less than 2% of inter-spike intervals were shorter than 2 ms. We also calculated a spike quality index, defined as the ratio between the peak amplitude of the waveform and the average variance, calculated using the channel with the largest amplitude. Cells were only included in the analysis if they had a spike quality index greater than 2.5.

III.3.5. Histology

At the conclusion of the experiment, animals were deeply anesthetized with euthasol and perfused through the heart with 4% paraformaldehyde. Brains were extracted and left in 4% paraformaldehyde for at least 24 hours before slicing. Brains were sliced under phosphate-buffered saline on a vibratome with a slice thickness of 100 μm. Brain slices were imaged with a fluorescent microscope (Axio Imager 2, Carl Zeiss) with a 2.5x objective. Expression of transgenes was verified by the presence of fluorescence. To determine the locations of our fiber implants, we manually registered each histology slice to the corresponding coronal section in the Allen Mouse Common Coordinate Framework (Common Coordinate Framework v.3, c 2015 Allen Institute for Brain Science, Allen Brain Atlas API, available from http://brain-map.org/api/index.html).

III.3.6. Analysis of behavioral data

To quantify how well a subject was able to detect the presence of a pure tone signal, we calculated the subject's sensitivity from the hit rate and false alarm rate,

as follows:

$$d' = z(\text{Hit Rate}) - z(\text{False Alarm Rate})$$

Z in this case is the inverse cumulative distribution function of the standard normal. Hit rates were calculated as a percentage of trials containing the signal where the mouse correctly reported the signal's presence. False alarm rates were calculated as a percentage of trials not containing the signal where the mouse incorrectly reported the signal's presence.

III.3.7. Statistical Analysis

To test for statistically significant effects across subjects (e.g. changes in sensitivity elicited by PV or SOM inactivation), we used the non-parametric Wilcoxon rank-sum test, because the data were rarely normally distributed and of equal variance. To test for significant effects within subjects (e.g. testing effects of laser inactivation of one cell type), we used the non-parametric Wilcoxon signed-rank test. To test for significant correlations between two continuous variables, we computed a least-squares linear regression. A Bonferroni correction was applied in situations where multiple comparisons were made.

III.4. Results

III.4.1. Detection of acoustic signals in noise

To investigate the neuronal mechanisms involved in the detection of acoustic signals in background noise, we trained mice to perform a signal detection task where they had to report the presence or absence of a pure tone signal (8 kHz) immersed in an amplitude modulated noise masker (Fig. III.1A, B). Mice successfully learned

this task, and their ability to detect the pure tone signal was highest for trials where the signal-to-noise ratio (SNR) was the largest (Fig. III.1C,D).

Consistent with the effect of comodulation masking release (Sollini and Chadderton, 2016), sensitivity to the pure tone signal was lower when the noise masker had a narrow bandwidth (0.25 octaves) compared to a broad bandwidth (white noise), despite the greater power contained within the broadband noise masker (median across animals $d' = 0.797$ for narrowband masker, median $d' = 1.190$ for broadband, $p = 4.67 \times 10^{-6}$, Wilcoxon signed-rank test, $N = 48$ mice). Hit rates and false alarm rates were both significantly higher when the masker was narrowband rather than broadband (median narrowband hit rate = 81%, median broadband hit rate = 65%, $p = 3.38 \times 10^{-13}$; median narrowband false alarm rate = 46%, median broadband hit rate = 21%, $p = 5.11 \times 10^{-13}$; Wilcoxon signed-rank test). This result indicates that mice reported the presence of tones more often when the masker was narrowband, even when the tone was not present. Yet, because the improvements in hit rate for narrowband masker trials were not as high as the increases in false alarms, the overall performance was lower compared to trials with a broadband masker. Overall, these results show that mice can successfully perform a signal-in-noise detection task, and that detection performance depends on the conditions of the stimulus (SNR and bandwidth of the masker).

III.4.2. Inactivation of the auditory cortex impairs detection of signals in noise

To determine the contribution of auditory cortical circuits to the detection of acoustic signals in background noise, we measured the animals' performance in the task described above while inactivating the auditory cortex bilaterally in

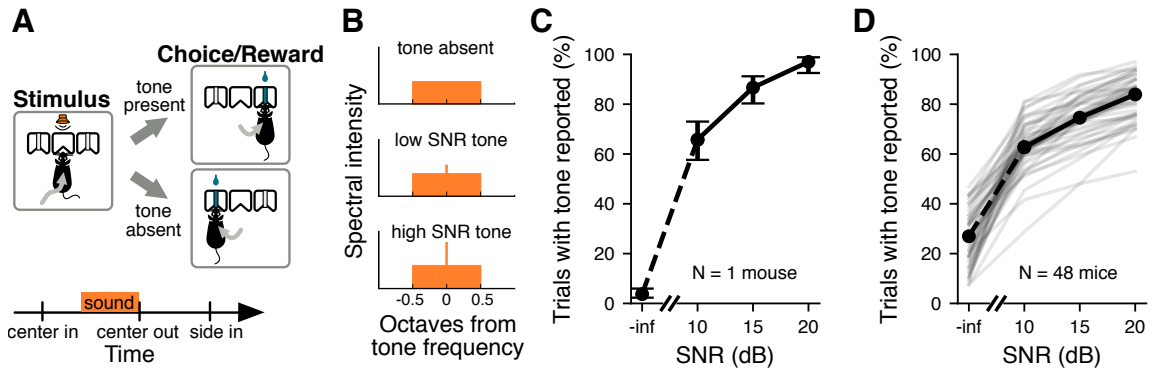

FIGURE III.1. Performance in a signal detection task.
(A), Schematic of the signal detection task. Mice had to correctly report the presence or absence of a pure tone signal to obtain a reward. **(B)**, Frequency spectra of sounds used during the signal detection task. **(C)**, Example psychometric curve showing performance of one mouse during one behavior session. Performance is averaged over all masker bandwidths presented. Error bars show 95% confidence intervals. **(D)**, Median psychometric curve (black line) for all mice trained in the signal detection task that achieved at least 60% accuracy ($N = 48$ mice). Psychometric curves for individual mice are shown in gray. Trials are pooled across all sessions. Performance is averaged over all masker bandwidths presented.

a subset of trials using optogentics. Mice expressing the light-gated ion channel channelrhodopsin-2 (ChR2) in parvalbumin-expressing inhibitory interneurons (PV^+) were trained in the task, and then implanted with optical fibers to deliver blue light to the auditory cortex in each hemisphere (Fig. III.2A). Histological analysis post-mortem was performed to ensure the fibers were located over the primary auditory cortex. Optogenetic activation of cortical PV+ cells has been shown to be a reliable method for reversibly silencing cortical circuits (Sachidhanandam et al., 2013; Glickfeld et al., 2013), allowing us to determine the effects cortical inactivation on signal detection in noise.

Bilateral inactivation of the primary auditory cortex during sound presentation impaired the performance of the mice in the detection task, reducing their sensitivity to the stimulus (Fig. III.3A; $p = 0.0117$, Wilcoxon signed rank test). While the

baseline performance of mice differed by bandwidth of the masker, as described in the previous section, the effects of optogenetic manipulation did not depend on masker bandwidth. Thus, we pooled trials across bandwidths for subsequent analysis. We found that the decrease in performance level during inactivation trials could not be explained simply by visual distraction from the laser used for optogenetics, because the effect of the laser on the sensitivity index (d') was significantly larger when the laser was directed at the auditory cortex than when it was directed away ($p = 0.0173$, Wilcoxon signed-rank test). Moreover, we found no correlation between the changes in sensitivity index from each laser location condition (Fig. III.3D; $p = 0.593$, $r = 0.224$, linear regression).

The decrease in sensitivity index observed during inactivation of the auditory cortex was largely the result of a decrease in hit rates (Fig. III.3B; $p = 0.0117$, Wilcoxon-signed rank test). Although auditory cortical inactivation also significantly reduced false alarm rates (Fig. III.3C; $p = 0.025$, Wilcoxon-signed rank test), this improvement was not sufficient to overcome the decrease in hit rates. The combination of a decrease in hit rate and a decrease in false alarm rate indicates that mice reported the presence of the pure tone signal less often when the auditory cortex was inactivated, regardless of whether the signal was present or not. As with the effect on sensitivity, these effects could not be explained by visual distraction, as the changes in hit rate or false alarm rate were not correlated between the conditions where the laser was directed at the auditory cortex or away (Fig. III.3E,F, hit rate: $p = 0.157$, $r = 0.710$; false alarm rate: $p = 0.589$, $r = 0.227$; linear regression). Moreover, the observed deficits during auditory cortex inactivation were not related to which port was associated with the presence or absence of the signal, as mice

trained to go to opposite sides to report the presence of the signal were all impaired in their ability to detect the signal (Fig. III.2B,C).

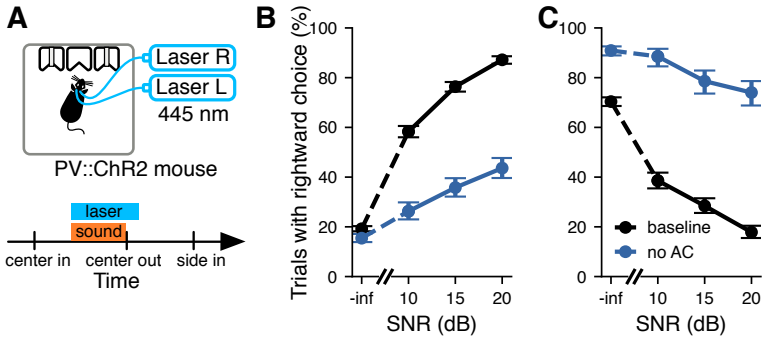

FIGURE III.2. Inactivation of the auditory cortex impairs performance in a signal detection task.
(A), Top: optogenetic stimulation in freely-moving PV::ChR2 mice. Laser activation of PV cells in the auditory cortex silences auditory cortical activity. Bottom: For a random 25% of trials, the laser turned on at the same time as the sound and lasted for 100 ms after the sound turned off. **(B)**, Example psychometric curve from one PV::ChR2 mouse trained to report the presence of the tone by going to the right. Activation of auditory cortical PV cells reduced the probability of the mouse reporting hearing the tone for all SNRs. Error bars show 95% confidence intervals. **(C)**, Like B, but for a PV::ChR2 mouse trained to go to the left to report the presence of the tone. As before, activation of auditory cortical PV cells reduced the probability of the tone being reported, despite the opposite action being required to report it.

To determine whether inactivation of the auditory cortex resulted in motor deficits during the task, we tested the effects of laser stimulation on the timing of the animals' motor output. Optogenetic inactivation of the auditory cortex did not significantly affect the amount of time mice spent sampling the sound before making their decision (Fig. III.4A; $p = 0.0925$, Wilcoxon signed-rank test), or the amount of time it took mice to reach the reward ports upon leaving the center port (Fig. III.4B; $p = 0.779$, Wilcoxon signed-rank test). Changes in sampling time and time to reward were not correlated between conditions where the laser was directed at auditory cortex or directed away, indicating that the effects of visual distraction

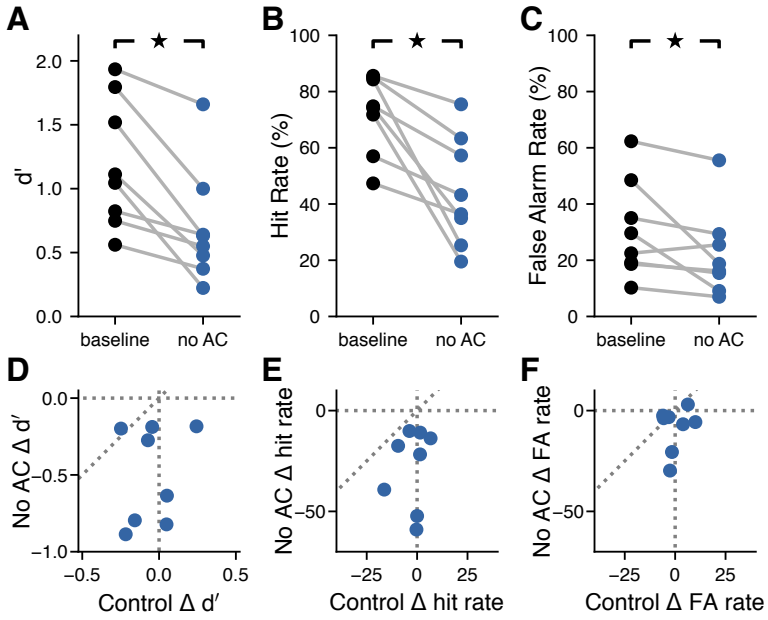

FIGURE III.3. The auditory cortex is important for detection of signals masked by noise.

(A), Silencing auditory cortex during the signal detection task significantly reduced sensitivity to the signal ($p = 0.0117$, Wilcoxon signed-rank test, $N = 8$ mice). **(B)**, Silencing auditory cortex during the signal detection task significantly reduced the hit rate ($p = 0.0117$, Wilcoxon signed-rank test). **(C)**, Silencing auditory cortex during the signal detection task significantly reduced the false alarm rate ($p = 0.025$, Wilcoxon signed-rank test). **(D)**, The effect of silencing the auditory cortex on d' was not correlated with the effect of visual distraction on d' ($p = 0.593$, $r = 0.224$, linear regression). **(E)**, The effect of silencing the auditory cortex on hit rate was not correlated with the effect of visual distraction on hit rate ($p = 0.157$, $r = 0.710$, linear regression). **(F)**, The effect of silencing the auditory cortex on false alarm rate was not correlated with the effect of visual distraction on false alarm rate ($p = 0.589$, $r = 0.227$, linear regression).

were unrelated to any effects brought about by inactivation of the auditory cortex (Fig. III.4C,D; sampling time: $p = 0.675$, $r = 0.176$; time to reward: $p = 0.686$, $r = -0.171$; linear regression). These results suggests that the effects of auditory cortical inactivation on performance in the signal detection task were the result of a perceptual deficit, not a motor deficit.

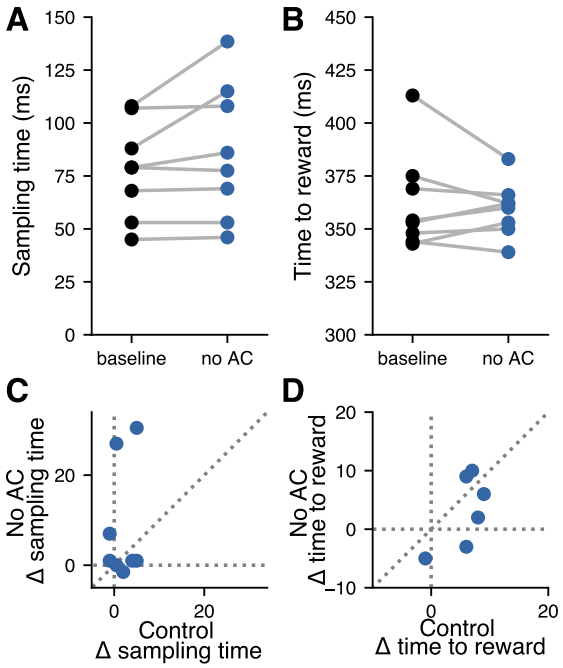

FIGURE III.4. Inactivation of auditory cortex does not affect timing of behavior. **(A)**, Silencing auditory cortex during the signal detection task did not affect time spent sampling the sound in the center port ($p = 0.0925$, Wilcoxon signed-rank test, $N = 8$ mice). **(B)**, Silencing auditory cortex during the signal detection task did not affect time spent moving toward the reward port ($p = 0.779$, Wilcoxon signed-rank test). **(C)**, The effect of silencing the auditory cortex on center port dwell time was not correlated to the effect of visual distraction on center port dwell time. ($p = 0.675$, $r = 0.176$, linear regression). **(D)**, The effect of silencing the auditory cortex on time spent obtaining reward was not correlated to the effect of visual distraction on time spent moving toward the reward port. ($p = 0.686$, $r = -0.171$, linear regression).

III.4.3. Cortical inhibitory neurons contribute to auditory signal detection in noise

To determine the extent to which distinct cortical inhibitory interneuron types are involved in auditory signal detection in noise, we measured the performance of animals in the detection task described above while perturbing the activity of either parvalbumin-expressing (PV^+) or somatostatin-expressing (SOM^+) neurons from the auditory cortex bilaterally. We trained mice that express the light-driven outward proton pump archaerhodopsin (ArchT) in either PV^+ or SOM^+ cells, and implanted these mice with optical fibers to enable delivering green light to the auditory cortex during the sound presentation in a subset of trials (Fig. III.5A, III.6A). Histological analysis post-mortem confirmed that the fibers were located over the primary auditory cortex. We also verified electrophysiologically that optogenetic inactivation of a particular inhibitory cell type using ArchT perturbs neural activity throughout the auditory cortex, resulting in an overall increase in sound-evoked responses of putative excitatory cells as expected from a decrease in inhibition ($N = 88 cells$, $p = 1.54 \times 10^{-6}$, Wilcoxon signed-rank test tested in a PV::ArchT mouse).

Optogenetic perturbation of either PV^+ or SOM^+ cells during sound presentation impaired performance of the task (Fig. III.5B, III.6B), reducing the sensitivity of the mice to the stimulus (Fig. III.5C, III.6C, PV::ArchT $p = 0.0046$, SOM::ArchT $p = 0.0051$, Wilcoxon signed-rank test). This reduction in performance could not be fully explained by visual distraction from the laser, as the majority of mice had larger deficits in sensitivity when the laser was directed at the auditory cortex rather than directed away (77% of PV::ArchT mice, 80% of SOM::ArchT mice), and there was no significant correlation between the changes in sensitivity

from these laser conditions (Fig. III.5F, III.6F; PV::ArchT $p = 0.609$, $r = 0.156$; SOM::ArchT $p = 0.546$, $r = 0.218$; linear regression).

We found that the reduction in sensitivity from perturbation of inhibitory interneurons was, for both cell types, explained by a reduction in hit rate (Fig. III.5D, III.6D, PV::ArchT $p = 0.033$, SOM::ArchT $p = 0.0051$, Wilcoxon signed-rank test), while false alarm rate was not significantly affected (Fig. III.5E, III.6E; PV::ArchT $p = 0.861$, SOM::ArchT $p = 0.878$, Wilcoxon signed-rank test). In PV::ArchT animals, neither hit rate nor false alarm rate was correlated between conditions where the laser was directed to the auditory cortex and directed away (Fig. III.5G,H; hit rate $p = 0.657$, $r = -0.136$; false alarm rate $p = 0.981$, $r = -0.0073$; linear regression), showing that the effects seen can not be explained by visual distraction In SOM::ArchT animals, we observed some degree of correlation between the laser directed to the auditory cortex and directed away, reaching statistical significance for hit rate but not false alarm rate (Fig. III.6G,H; hit rate $p = 0.049$, $r = 0.633$; false alarm rate $p = 0.072$, $r = 0.590$; linear regression). Nonetheless, the majority (70%) of SOM::ArchT animals had a greater effect on hit rate when the laser was directed at the auditory cortex, suggesting that visual distraction cannot fully account for the effects on hit rate. These results indicate that, contrary to our original hypothesis regarding different roles for distinct inhibitory neuron classes during signal detection, perturbing PV^+ or SOM^+ cell activity results in comparable effects on behavioral output in the signal-in-noise detection task describe here.

To test whether perturbation of either PV^+ or SOM^+ cells from the auditory cortex resulted any in motor deficits during the task, we quantified changes in the timing of the animals' motor output during laser trials. Perturbation of SOM^+, but not PV^+, increased the amount of time mice spend sampling sound, although the

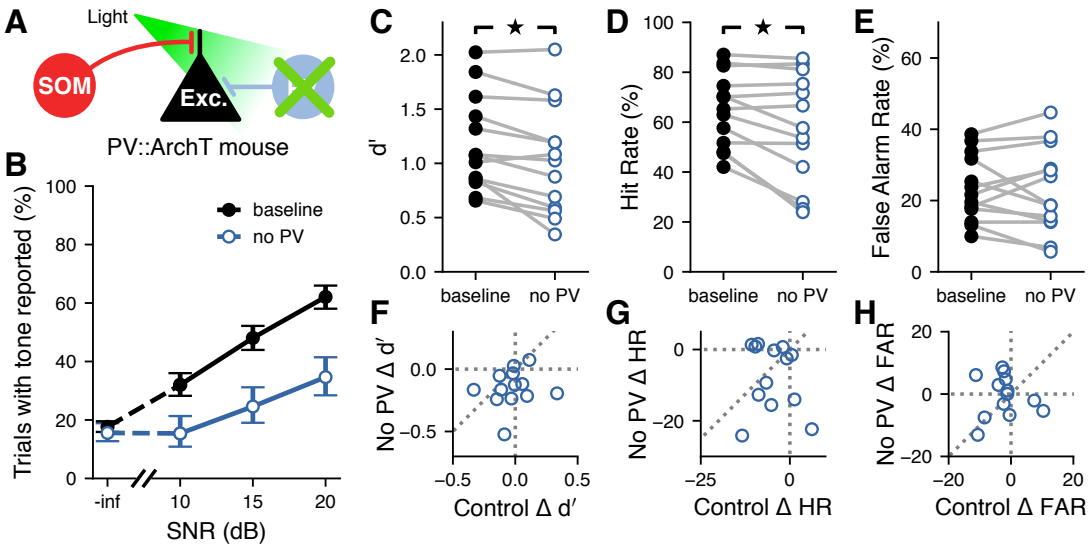

FIGURE III.5. Contributions of PV$^+$ cells to auditory signal detection. **(A)**, Inactivation of PV$^+$ cells during the signal detection task. **(B)**, Example psychometric curve from one PV::ArchT mouse. Inactivation of auditory cortical PV$^+$ cells decreased the probability of the mouse reporting hearing the signal when it was present, though false alarm rate was unaffected. Error bars show 95% confidence intervals. **(C)**, Inactivating auditory cortical PV$^+$ cells during the signal detection task significantly reduced sensitivity to the signal ($p = 0.0046$, Wilcoxon signed-rank test, $N = 13$ mice). **(D)**, Inactivating auditory cortical PV$^+$ cells during the signal detection task significantly reduced the hit rate ($p = 0.033$, Wilcoxon signed-rank test). **(E)**, Inactivating auditory cortical PV$^+$ cells during the signal detection task did not significantly affect the false alarm rate ($p = 0.861$, Wilcoxon signed-rank test). **(F)**, The effect of inactivating auditory cortical PV$^+$ cells on d' was not correlated with the effect of visual distraction on d' ($p = 0.609$, $r = 0.156$, linear regression). **(G)**, The effect of inactivating auditory cortical PV$^+$ cells on hit rate was not correlated with the effect of visual distraction on hit rate ($p = 0.657$, $r = -0.136$, linear regression). **(H)**, The effect of inactivating auditory cortical PV$^+$ cells on false alarm rate was not correlated with the effect of visual distraction on false alarm rate ($p = 0.981$, $r = -0.0073$, linear regression).

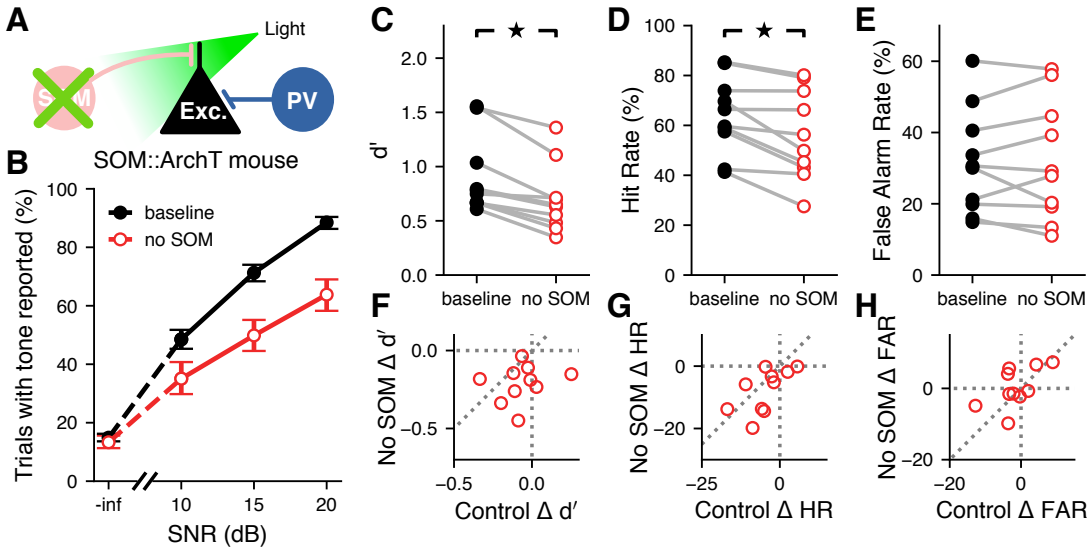

FIGURE III.6. Contributions of SOM$^+$ cells to auditory signal detection. **(A)**, Inactivation of SOM$^+$ cells during the signal detection task. **(B)**, Example psychometric curve from one SOM::ArchT mouse. Inactivation of auditory cortical SOM$^+$ cells reduced the probability of the mouse reporting hearing the signal when it was present, though false alarm rate was unaffected. Error bars show 95% confidence intervals. **(C)**, Inactivating auditory cortical SOM$^+$ cells during the signal detection task significantly reduced sensitivity to the signal ($p = 0.0051$, Wilcoxon signed-rank test, $N = 10$ mice). **(D)**, Inactivating auditory cortical SOM$^+$ cells during the signal detection task significantly reduced hit rate ($p = 0.0051$, Wilcoxon signed-rank test). **(E)**, Inactivating auditory cortical SOM$^+$ cells during the signal detection task did not significantly affect the false alarm rate ($p = 0.721$, Wilcoxon signed-rank test). **(F)**, The effect of inactivating auditory cortical SOM$^+$ cells on d' was not correlated with the effect of visual distraction on d' ($p = 0.543$, $r = 0.219$, linear regression). **(G)**, The effect of inactivating auditory cortical SOM$^+$ cells on hit rate was correlated with the effect of visual distraction on hit rate ($p = 0.047$, $r = 0.638$, linear regression). **(H)**, The effect of inactivating auditory cortical SOM$^+$ cells on false alarm rate was not correlated with the effect of visual distraction on false alarm rate ($p = 0.057$, $r = 0.616$, linear regression).

effect sizes were very small in both cases (Fig. III.7A,E; PV::ArchT $p = 0.065$, 1% change, SOM::ArchT $p = 0.005$, 3.7% change, median change of 3 ms). The effects on sampling time in PV::ArchT animals were strongly correlated between conditions with the laser directed to the auditory cortex and directed away (Fig. III.7B, $p = 0.0017$, $r = 0.780$, linear regression), suggesting that any effect on sampling time that results from PV+ cell perturbation may be a result of distraction by light. In contrast, there was no correlation between these laser conditions in SOM::ArchT animals (Fig. III.7F, $p = 0.901$, $r = 0.045$, linear regression), suggesting that the small effects observed from SOM^+ cell perturbation are not simply the result of visual distraction by the laser. Last, the time mice took to reach the reward ports was minimally affected by perturbation of PV^+ cells (Fig. III.7C, $p = 0.0029$, 1.8% change) and did not reach statistical significance in SOM::ArchT mice (Fig. III.7G, $p = 0.203$, 1.4% change). Moreover, there was no correlation between conditions where the laser was directed to the auditory cortex *vs* away in either mouse strain (Fig. III.7D,H; PV::ArchT $p = 0.901$, $r = 0.038$; SOM::ArchT $p = 0.470$, $r = 0.259$; linear regression). These results indicate that perturbation of PV^+ or SOM^+ cell activity does not result in substantial motor deficits, suggesting that the effects on behavioral output are likely perceptual in nature.

III.5. Discussion

In this study, we investigated how different sources of inhibition within the auditory cortex contribute to the perception of a pure tone stimulus immersed in background noise. Previous studies have found population-level noise-invariant representations of masked auditory stimuli in the auditory cortex (Christison-Lagay et al., 2017), and discovered that the auditory cortex plays a role in mediating signal

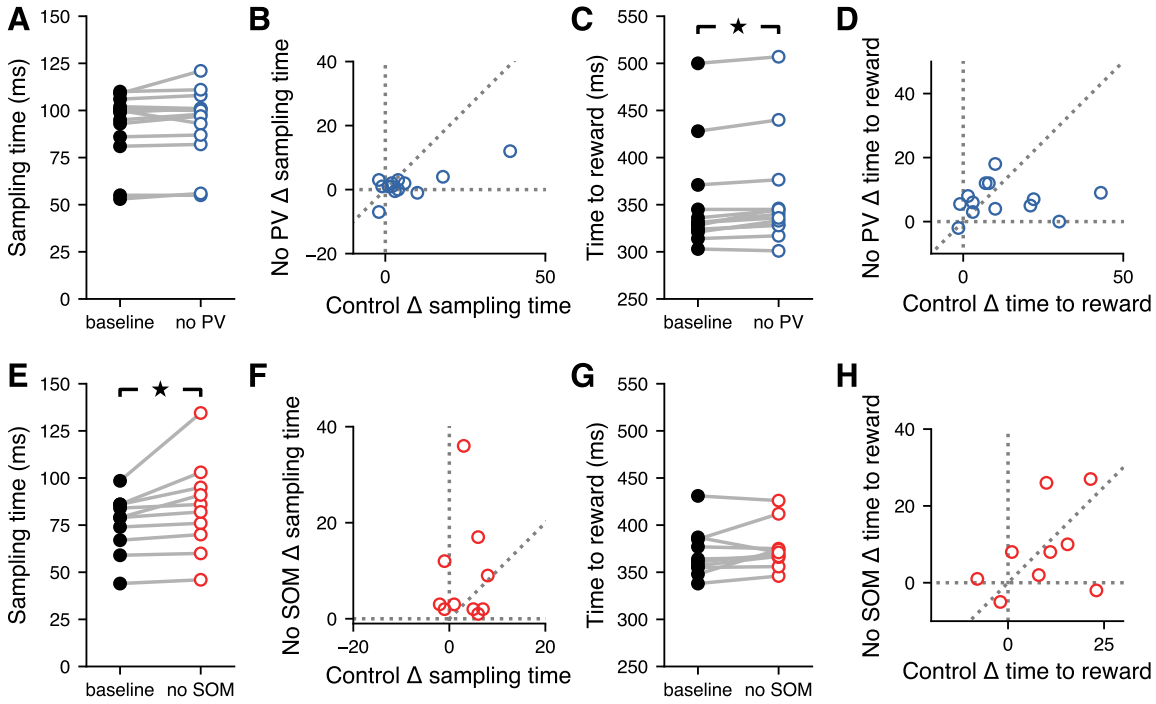

FIGURE III.7. Inactivation of distinct inhibitory neuron types does not affect timing of behavior.

(A), Inactivating auditory cortical PV$^+$ cells during the signal detection task did not affect time spent sampling the sound in the center port ($p = 0.065$, Wilcoxon signed-rank test). **(B)**, The effect of inactivating auditory cortical PV$^+$ cells on sampling time was correlated with the effect of visual distraction on center port dwell time ($p = 0.0017$, $r = 0.780$, linear regression). **(C)**, Inactivating auditory cortical PV$^+$ cells during the signal detection task led to a small (1.7%) but statistically significant increase in time spent obtaining a reward ($p = 0.0029$, Wilcoxon signed-rank test). **(D)**, The effect of inactivating auditory cortical PV$^+$ cells on time spent obtaining a reward was not correlated with the effect of visual distraction on time spent obtaining a reward ($p = 0.901$, $r = 0.038$, linear regression). **(E)**, Inactivating auditory cortical SOM$^+$ cells during the signal detection task significantly increased time spent sampling the sound in the center port, leading to a 12% increase in sampling time ($p = 0.005$, Wilcoxon signed-rank test). **(F)**, The effect of inactivating auditory cortical SOM$^+$ cells on sampling time was not correlated with the effect of visual distraction on center port dwell time ($p = 0.848$, $r = 0.070$, linear regression). **(G)**, Inactivating auditory cortical SOM$^+$ cells during the signal detection task did not affect time spent obtaining a reward ($p = 0.202$, Wilcoxon signed-rank test). **(H)**, The effect of inactivating auditory cortical SOM$^+$ cells on time spent obtaining a reward was not correlated with the effect of visual distraction on time spent obtaining a reward ($p = 0.452$, $r = 0.269$, linear regression).

detection (Sollini and Chadderton, 2016). Consistent with these studies, we found that optogenetically silencing the auditory cortex during sound presentation resulted in mice becoming less likely to report the presence of narrowband signals, confirming that the auditory cortex plays an important role in identifying behaviorally relevant signals in noisy acoustic environments. Interestingly, silencing the auditory cortex also reduced the rate at which false alarms occurred, but did not affect the timing or direction of movement. This suggests that the observed effects on behavior were perceptual in nature rather than motor, and that outputs from the auditory cortex are partially responsible for the perception of hallucinatory stimuli. Furthermore, inactivation of either PV^+ or SOM^+ cells during sound presentation created a deficit in performance specifically by decreasing hit rates, indicating that perturbing inhibitory auditory cortical circuits disrupts the outputs that carry information about the presence of signals.

Contrary to the expectation that detecting loud stimuli would rely less on auditory cortical circuits, we observed comparable effects for low and high SNR when inactivating the auditory cortex. Thus, the idea that a partially active auditory cortex is sufficient to detect loud signals does not explain the limited ability of mice to separate signals from noise during our perturbation of cortical circuits. Instead, our results are better explained by the assumption that we are fully silencing the auditory cortex, but some residual processing is preserved in other auditory areas.

Our results indicate that activating and inactivating PV^+ cells have very similar effects on behavior. While a decrease in sensitivity (d') is an expected result of any perturbation of normal auditory cortical activity, perturbing PV^+ cells in either direction resulted in the same effect on hit rate, raising the question of why opposite manipulations of PV^+ cells would result in similar effects on signal detection. Two

mechanisms likely contribute to the ability to detect signals in noise: suppression of responses to broadband noise and amplification of responses to narrowband signals. The former has been shown to be mediated in part by cortical inhibition (Lakunina et al., 2020), while the latter may be performed by the auditory cortex or inherited from upstream areas. The auditory cortex could use a combination of these mechanisms to determine the presence or absence of signals and pass this information to downstream areas. Thus, silencing the auditory cortex entirely (through the activation of PV^+ cells) would lead to a decrease both in hit rate and false alarm rate because the neural signals triggering the perception of auditory stimuli are failing to travel to downstream areas. In contrast, inactivation of PV^+ cells would disrupt the auditory cortical circuits needed to suppress responses to broadband noise, leading to a decrease in hit rate (as with activation of PV^+ cells), but may not affect the circuits amplifying narrowband signals, leading to no change in false alarm rate, unlike when activating PV^+ cells. Consistent with these ideas, we observed that activation of PV^+ cells led to a decrease in false alarm rate, while inactivation of PV^+ cells did not have an effect on false alarm rate.

Our experiment relied on inactivating PV^+ cells with ArchT to determine the effect this cell type plays on separating auditory signals from noise. Under some circumstances, laser inactivation of PV^+ with ArchT may be ineffective at reducing PV^+ firing rates due to recurrent network effects causing a paradoxical increase in both PV^+ and excitatory cell responses (Moore et al., 2018). However, an increase in excitatory activity, which we observed in electrophysiolgical recordings in PV::ArchT animals, is indicative of a perturbation of the normal function of PV^+ cells in cortical circuits, and the behavioral effects presented here are therefore the result of disrupting the normal function of PV^+ cells during detection of auditory signals.

An additional concern when manipulating neural activity with optogenetics is that activation and inactivation of a particular cell type may not produce entirely opposite effects on physiological responses due to the nonlinearities produced by thresholds or saturation of neural activity (Phillips and Hasenstaub, 2016). While these caveats may partly explain our observation that activation and inactivation of PV^+ cells result in similar decreases in hit rate, opposite effects on neural responses do not necessarily result in opposite effects on behavior. As described above, it is plausible that both silencing the auditory cortex entirely (through the activation of PV^+ cells) and disrupting inhibitory auditory cortical circuits (through the inactivation of PV^+ cells) would result in a deficit in signal detection that would lead to a decrease in hit rate.

This study sought to determine whether PV^+ and SOM^+ cells have different contributions to the ability to detect a behaviorally relevant signal immersed in broadband noise. Previous studies have shown that PV^+ and SOM^+ cells have different contributions to lateral inhibition and surround suppression (Adesnik et al., 2012; Kato et al., 2017; Lakunina et al., 2020), processes that we hypothesized would be important to the suppression of responses to broadband noise. Despite this, we found that inactivation of either PV^+ or SOM^+ cells had, on average, similar effects on behavioral output, in both cases leading to a reduction in hit rate and no effect on false alarm rate. This may indicate that, if background subtraction occurs in the auditory cortex, the sources of inhibition underlying this mechanism are not split along the broadly-defined gene-expression categories we studied. It is also possible that PV^+ and SOM^+ cells play different roles in the implementation of the circuit mechanisms that give rise to noise-invariant responses, but the perturbation of their activity has widespread effects on the auditory cortex which degrade performance

in an auditory signal detection task. For instance, perturbation of either PV^+ or SOM^+ cells may increase spontaneous activity in the auditory cortex and worsen the signal-to-noise ratio of responses to auditory stimuli. Spontaneous activity in the auditory cortex is modulated to increase the signal-to-noise ratio during behavioral engagement in signal detection tasks (Buran et al., 2014; Carcea et al., 2017), and disruption of the peripheral auditory system hinders signal detection by increasing signal-to-noise ratio in the auditory cortex (Resnik and Polley, 2021). As a result, inactivation of PV^+ or SOM^+ cells may have further-reaching effects than the disruption of circuits responsible for the removal of background noise. That said, our inactivation experiments showed that cortical inhibition plays an important role in the cortical computations performed by the auditory cortex to process sound stimuli.

CHAPTER IV

CONCLUSION

This dissertation attempted to answer following questions: what are the mechanisms of global integration in the auditory cortex, and are these mechanisms useful for auditory signal detection? The work presented here furthers our understanding of the auditory system and made progress in addressing these questions. In Chapter II, I dissected inhibitory cortical circuits in the auditory cortex to determine the extent to which spectral surround suppression, a form of global integration, is affected by different types of inhibitory inputs. In Chapter III, I presented a behavioral task that we used to determine if the sources of inhibition mediating surround suppression also affect the perception of signals immersed in background noise.

IV.1. Cortical circuits mediating spectral surround suppression

My results in Chapter II reveal that a large proportion of auditory cortical excitatory cells exhibit suppression of activity by their spectral surround. As a result of this phenomenon, neural responses to broadband stimuli, such as many naturally occurring types of acoustic noise, are reduced. I therefore posit that spectral surround suppression of neural responses can be used by the auditory system to filter out background noise while transmitting narrowband signals. The work in Chapter II identified a role of SOM^+ cells in the implementation of this integration of acoustic features for noise reduction, while PV^+ cells had comparatively small contributions to the phenomenon of surround suppression. Together with previous studies finding a similar role for SOM^+ cells in mediating surround suppression in

the visual cortex (Adesnik et al., 2012), our findings provide evidence of common circuit motifs repeated in the sensory cortex. These repeated cortical circuits may be indicative of a common mechanism implemented by the sensory cortex to isolate signals from noise.

IV.2. The auditory cortex mediates auditory signal detection

My results in Chapter III reveal that information output from the auditory cortex is important to the ability to make decisions on the presence or absence of behaviorally relevant signals in a noisy sound stimulus. My findings were consistent with previous studies showing population-level representations of masked auditory stimuli in the primary auditory cortex (Carcea et al., 2017), indicating that separation between representations of signals and noise already exists on this level of the auditory pathway. Furthermore, inactivating cortical inhibitory cells creates deficits in an animal's ability to detect signals and ignore noise. Together with previous studies finding that noise-invariant sound responses first emerge in the auditory cortex (Rabinowitz et al., 2013), these findings provide evidence of an auditory cortical mechanism for signal detection. The impact of inactivation of auditory cortical inhibition on performance in our signal detection task implies the existence of an inhibitory circuit within the primary auditory cortex that may broadly filter out stimuli fitting the typical statistics of natural noise.

IV.3. Do auditory cortical circuits mediate signal detection?

The results from Chapter II and III together show that cortical inhibition is important both for producing neural responses that are suppressed by broadband noise and for detecting narrowband signals immersed in broadband noise. It is

plausible that these functions are related to each other, as detection of narrowband stimuli in a background of broadband environmental noise would likely require some form of inhibition that suppresses responses to such noise. Nonetheless, the combination of these two results does not directly implicate cortical surround suppression in playing a role in detection of auditory signals. Further study is required to directly link these two results and would require recording responses from the auditory cortex while animals perform the auditory signal detection task. Such an experiment would allow us to directly investigate the neural computations taking place in the auditory cortex that allow for the separation of auditory stimuli into relevant signals and background noise. That said, the results of the experiments done in Chapter III do show the importance of auditory cortical inhibition in auditory signal detection, with the results from Chapter II providing a plausible mechanism for how the auditory cortex achieves the separation of signal and noise. The results of this dissertation advance the field of auditory neuroscience by demonstrating that cortical inhibition plays a role in signal detection and providing a possible mechanism by which cortical inhibition aids in suppression of responses to noise.

REFERENCES CITED

Abbas PJ (1981) Auditory-nerve fiber responses to tones in a noise masker. *Hearing Research* 5:69–80.

Abeles M, Goldstein MH (1972) Responses of single units in the primary auditory cortex of the cat to tones and to tone pairs. *Brain Research* 42:337–352.

Adesnik H, Bruns W, Taniguchi H, Huang ZJ, Scanziani M (2012) A neural circuit for spatial summation in visual cortex. *Nature* 490:226–231.

Ayaz A, Saleem A, Schölvinck M, Carandini M (2013) Locomotion Controls Spatial Integration in Mouse Visual Cortex. *Current Biology* 23:890–894.

Berg BG (2004) A temporal model of level-invariant, tone-in-noise detection. *Psychological Review* 111:914–930.

Blackwell JM, Geffen MN (2017) Progress and challenges for understanding the function of cortical microcircuits in auditory processing. *Nature Communications* 8:2165.

Boucsein C, Nawrot MP, Schnepel P, Aertsen A (2011) Beyond the cortical column: Abundance and physiology of horizontal connections imply a strong role for inputs from the surround.

Buran BN, von Trapp G, Sanes DH (2014) Behaviorally gated reduction of spontaneous discharge can improve detection thresholds in auditory cortex. *Journal of Neuroscience* 34:4076–4081.

Carcea I, Insanally MN, Froemke RC (2017) Dynamics of auditory cortical activity during behavioural engagement and auditory perception. *Nature Communications* 8.

Carruthers IM, Laplagne DA, Jaegle A, Briguglio JJ, Mwilambwe-Tshilobo L, Natan RG, Geffen MN (2015) Emergence of invariant representation of vocalizations in the auditory cortex. *Journal of Neurophysiology* 114:2726–2740.

Christison-Lagay KL, Bennur S, Cohen YE (2017) Contribution of spiking activity in the primary auditory cortex to detection in noise. *Journal of Neurophysiology* 118:3118–3131.

Costalupes JA (1985) Representation of tones in noise in the responses of auditory nerve fibers in cats. I. Comparison with detection thresholds. *Journal of Neuroscience* 5:3261–3269.

Glickfeld LL, Histed MH, Maunsell JH (2013) Mouse primary visual cortex is used to detect both orientation and contrast changes. *Journal of Neuroscience* 33:19416–19422.

Han X, Chow BY, Zhou H, Klapoetke NC, Chuong A, Rajimehr R, Yang A, Baratta MV, Winkle J, Desimone R, Boyden ES (2011) A High-Light Sensitivity Optical Neural Silencer: Development and Application to Optogenetic Control of Non-Human Primate Cortex. *Frontiers in Systems Neuroscience* 5:18.

Kadir SN, Goodman DFM, Harris KD (2014) High-dimensional cluster analysis with the masked EM algorithm. *Neural computation* 26:2379–94.

Kanold PO, Nelken I, Polley DB (2014) Local versus global scales of organization in auditory cortex.

Kato HK, Asinof SK, Isaacson JS (2017) Network-Level Control of Frequency Tuning in Auditory Cortex. *Neuron* 95:412–423.e4.

Kepecs A, Fishell G (2014) Interneuron cell types are fit to function.

Kuchibhotla KV, Gill JV, Lindsay GW, Papadoyannis ES, Field RE, Sten TAH, Miller KD, Froemke RC (2017) Parallel processing by cortical inhibition enables context-dependent behavior. *Nature Neuroscience* 20:62–71.

Kvitsiani D, Ranade S, Hangya B, Taniguchi H, Huang JZ, Kepecs A (2013) Distinct behavioural and network correlates of two interneuron types in prefrontal cortex. *Nature* 498:363–366.

Kwan AC, Dan Y (2012) Dissection of cortical microcircuits by single-neuron stimulation in vivo. *Current Biology* 22:1459–1467.

Lakunina AA, Nardoci MB, Ahmadian Y, Jaramillo S (2020) Somatostatin-expressing interneurons in the auditory cortex mediate sustained suppression by spectral surround. *Journal of Neuroscience* 40:3564–3575.

Levy RB, Reyes AD (2011) Coexistence of lateral and Co-Tuned inhibitory configurations in cortical networks. *PLoS Computational Biology* .

Levy RB, Reyes AD (2012) Spatial profile of excitatory and inhibitory synaptic connectivity in mouse primary auditory cortex. *Journal of Neuroscience* .

Li H, Liang F, Zhong W, Yan L, Mesik L, Xiao Z, Tao HW, Zhang LI (2019) Synaptic Mechanisms for Bandwidth Tuning in Awake Mouse Primary Auditory Cortex. *Cerebral Cortex* 29:2998–3009.

Li Ly, Xiong XR, Ibrahim LA, Yuan W, Tao HW, Zhang LI (2015) Differential Receptive Field Properties of Parvalbumin and Somatostatin Inhibitory Neurons in Mouse Auditory Cortex. *Cerebral Cortex* 25:1782–1791.

Li Ly, Ji Xy, Liang F, Li Yt, Xiao Z, Tao HW, Zhang LI (2014) A Feedforward Inhibitory Circuit Mediates Lateral Refinement of Sensory Representation in Upper Layer 2/3 of Mouse Primary Auditory Cortex. *The Journal of Neuroscience* 34:13670–13683.

Liang F, Li H, Chou Xl, Zhou M, Zhang NK, Xiao Z, Zhang KK, Tao HW, Zhang LI (2019) Sparse Representation in Awake Auditory Cortex: Cell-type Dependence, Synaptic Mechanisms, Developmental Emergence, and Modulation. *Cerebral Cortex* .

Ma Y, Hu H, Berrebi AS, Mathers PH, Agmon A (2006) Distinct Subtypes of Somatostatin-Containing Neocortical Interneurons Revealed in Transgenic Mice. *Journal of Neuroscience* 26:5069–5082.

Mao J, Carney LH (2015) Tone-in-Noise Detection Using Envelope Cues: Comparison of Signal-Processing-Based and Physiological Models. *JARO - Journal of the Association for Research in Otolaryngology* 16:121–133.

Mesgarani N, David SV, Fritz JB, Shamma SA (2014) Mechanisms of noise robust representation of speech in primary auditory cortex. *Proceedings of the National Academy of Sciences of the United States of America* 111:6792–7.

Metherate R, Kaur S, Kawai H, Lazar R, Liang K, Rose HJ (2005) Spectral integration in auditory cortex: Mechanisms and modulation. *Hearing Research* 206:146–158.

Moore AK, Wehr M (2013) Parvalbumin-Expressing Inhibitory Interneurons in Auditory Cortex Are Well-Tuned for Frequency. *Journal of Neuroscience* 33:13713–13723.

Moore AK, Weible AP, Balmer TS, Trussell LO, Wehr M (2018) Rapid Rebalancing of Excitation and Inhibition by Cortical Circuitry. *Neuron* 97:1341–1355.e6.

Moore RC, Lee T, Theunissen FE (2013) Noise-invariant Neurons in the Avian Auditory Cortex: Hearing the Song in Noise. *PLoS Computational Biology* 9:e1002942.

Naka A, Veit J, Shababo B, Chance RK, Risso D, Stafford D, Snyder B, Egladyous A, Chu D, Sridharan S, Mossing DP, Paninski L, Ngai J, Adesnik H (2019) Complementary networks of cortical somatostatin interneurons enforce layer specific control. *eLife* 8:e43696.

Natan RG, Briguglio JJ, Mwilambwe-Tshilobo L, Jones SI, Aizenberg M, Goldberg EM, Geffen MN (2015) Complementary control of sensory adaptation by two types of cortical interneurons. *eLife* 4.

Natan RG, Rao W, Geffen MN (2017) Cortical Interneurons Differentially Shape Frequency Tuning following Adaptation. *Cell Reports* 21:878–890.

Nelken I, Prut Y, Vaadia E, Abeles M (1994) Population responses to multifrequency sounds in the cat auditory cortex: One- and two-parameter families of sounds. *Hearing Research* 72:206–222.

Nelken I, Rotman Y, Bar Yosef O (1999) Responses of auditory-cortex neurons to structural features of natural sounds. *Nature* 397:154–7.

O'Connor KN, Yin P, Petkov CI, Sutter ML (2010) Complex Spectral Interactions Encoded by Auditory Cortical Neurons: Relationship Between Bandwidth and Pattern. *Frontiers in Systems Neuroscience* 4:145.

Pfeffer CK, Xue M, He M, Huang ZJ, Scanziani M (2013) Inhibition of inhibition in visual cortex: The logic of connections between molecularly distinct interneurons. *Nature Neuroscience* 16:1068–1076.

Phillips EAK, Schreiner CE, Hasenstaub AR (2017) Cortical Interneurons Differentially Regulate the Effects of Acoustic Context. *Cell reports* 20:771–778.

Phillips EA, Hasenstaub AR (2016) Asymmetric effects of activating and inactivating cortical interneurons. *eLife* 5.

Rabinowitz N, Willmore B, Schnupp J, King A (2013) Constructing Noise-Invariant Representations of Sound in the Auditory Pathway. *PLoS Biol* 11:e1001710.

Ralli M, Greco A, De Vincentiis M, Sheppard A, Cappelli G, Neri I, Salvi R (2019) Tone-in-noise detection deficits in elderly patients with clinically normal hearing. *American Journal of Otolaryngology - Head and Neck Medicine and Surgery* 40:1–9.

Rauschecker JP, Tian B (2004) Processing of Band-Passed Noise in the Lateral Auditory Belt Cortex of the Rhesus Monkey. *Journal of Neurophysiology* 91:2578–2589.

Resnik J, Polley DB (2021) Cochlear neural degeneration disrupts hearing in background noise by increasing auditory cortex internal noise. *Neuron* 109:984–996.e4.

Rudy B, Fishell G, Lee S, Hjerling-Leffler J (2011) Three groups of interneurons account for nearly 100GABAergic neurons. *Developmental Neurobiology* 71:45–61.

Sachidhanandam S, Sreenivasan V, Kyriakatos A, Kremer Y, Petersen CC (2013) Membrane potential correlates of sensory perception in mouse barrel cortex. *Nature Neuroscience* 16:1671–1677.

Schneider DM, Woolley SM (2013) Sparse and Background-Invariant Coding of Vocalizations in Auditory Scenes. *Neuron* 79:141–152.

Sollini J, Chadderton P (2016) Comodulation enhances signal detection via priming of auditory cortical circuits. *Journal of Neuroscience* 36:12299–12311.

Weible AP, Liu C, Niell CM, Wehr M (2014a) Auditory cortex is required for fear potentiation of gap detection. *Journal of Neuroscience* 34:15437–15445.

Weible AP, Moore AK, Liu C, Deblander L, Wu H, Kentros C, Wehr M (2014b) Perceptual gap detection is mediated by gap termination responses in auditory cortex. *Current Biology* 24:1447–1455.